

THE MANY FACES OF MARS

(NASA-CR-137432) THE MANY FACES OF MARS
(Jet Propulsion Lab.) 56 p HC \$3.75

874-21493

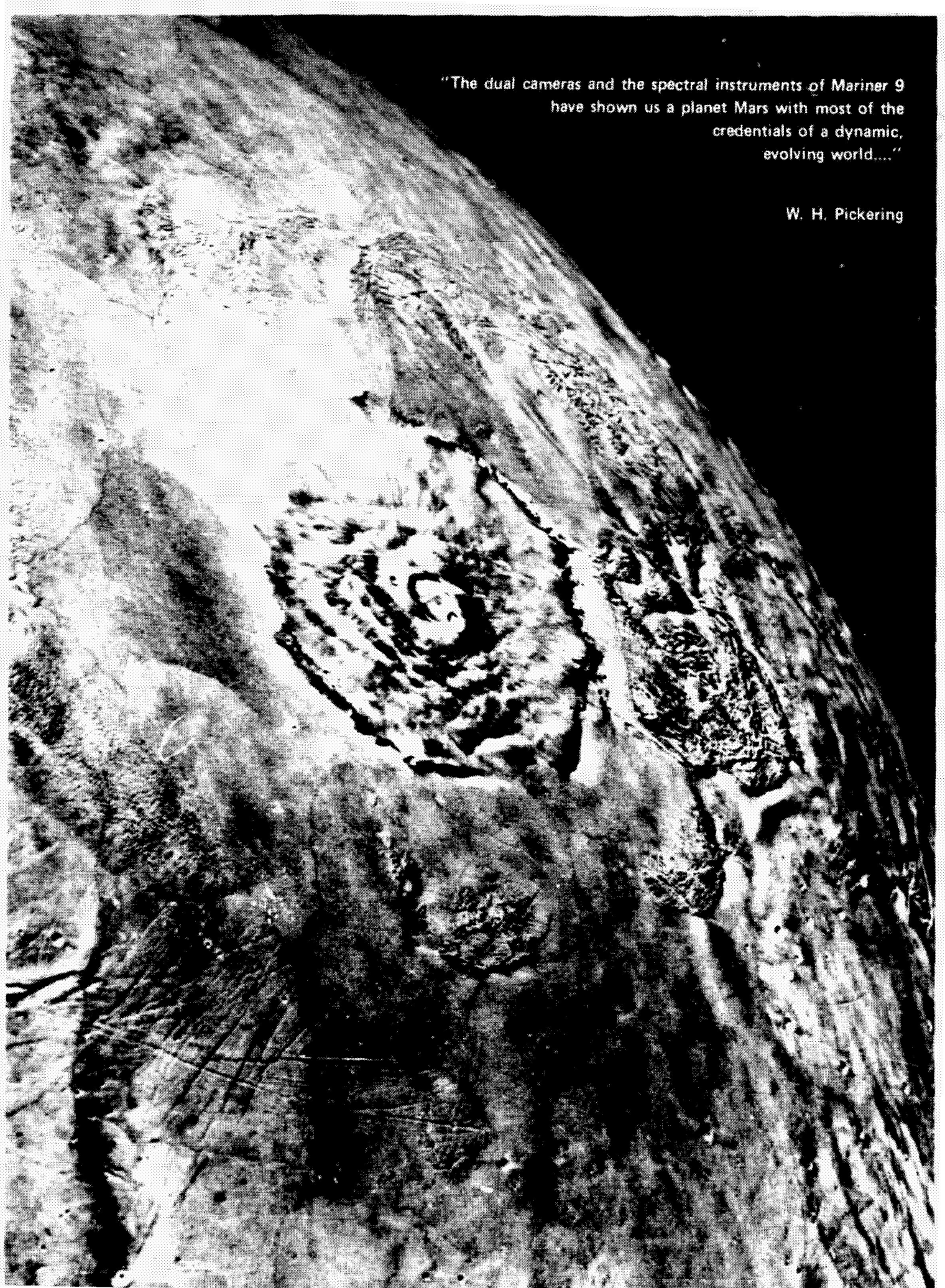
CSCL 03B

Unclassified
G3/30 36281



THE MANY FACES OF MARS

National Aeronautics and Space Administration
Jet Propulsion Laboratory/California Institute of Technology
Pasadena, California
Mariner Mars 1971 Project Office
JPL Technical Memorandum 33-654
December 1973



"The dual cameras and the spectral instruments of Mariner 9 have shown us a planet Mars with most of the credentials of a dynamic, evolving world...."

W. H. Pickering

FOREWORD

Perhaps no planet in our solar system has been more curiously regarded or aroused more speculation than Mars — from scientific theories about the canals, spring growth, the wave of darkening, and the possibility of some form of life, to the popular fictional fancy of little green men with intellects far more developed than those of earthlings.

Mariners 4, 6, and 7 in 1965 and 1969 provided man's first close look at Mars, but, because these spacecraft flew by the planet, the look was brief.

Mariner 9, the first to ever do so, orbited the planet. The spacecraft carried five scientific instruments and performed six scientific experiments. For 349 days, Mariner 9 transmitted a vast amount of data, including 7300 television pictures.

Here, then, in this document are some findings revealed by man's first long, close look at the "dynamic, evolving world" of Mars.

Mission Event Summary

Mariner 9 was launched from Cape Kennedy, Florida, on May 30, 1971, (Figs. 1 and 2) on a direct-ascent trajectory. The launch was deliberately aimed away from Mars to ensure that neither the unsterilized Centaur launch vehicle nor the spacecraft would impact Mars and contaminate the planet. When the spacecraft safely responded to commands after launch, its trajectory was altered on June 4 for Mars intercept on November 13, 1971. This trajectory-correction maneuver was performed with such accuracy that no other corrections were necessary for the entire 167-day flight to Mars (Fig. 3).

The objectives of the Mariner 9 mission were to photographically map the surface of the planet and to observe the dynamic characteristics of the surface and atmosphere from orbit for at least 90 days. To achieve these objectives, six experiments were carried on the spacecraft: television, ultraviolet spectrometer, infrared spectroscopy, infrared radiometry, S-band occultation, and celestial mechanics. Two experiments (S-band occultation and celestial mechanics) used the radio telemetry subsystem to gather data; the others required specially developed instruments (infrared radiometer, infrared interferometer spectrometer, ultraviolet spectrometer, and wide-and narrow-angle television cameras) mounted on the spacecraft's scan platform (Fig. 4), an articulating instrument mount with a pointing-selection capability of 215 degrees in azimuth and 69 degrees in elevation.

The acquisition of science data began shortly after launch by recording doppler and ranging information for the celestial mechanics experiment. In late September and early October, two star-observation sequences were conducted, using the television cameras and the ultraviolet spectrometer to provide calibration information for the scientific instruments and for the scan-platform pointing. Other instruments mounted on the scan platform also were tested for operational ability. Five days before arrival, recording and playback of Mars data were conducted over a two-day period, primarily to photometrically calibrate the television cameras; however, the data also gave some of the first close-up indications of the dust storm in progress on the planet. Some pictures also supplied data for accurately determining the positions of the two Martian satellites, Phobos and Deimos. This new information made it possible to photograph the satellites during orbital operations.

The first planetary science data were obtained three days before orbit insertion with a series of pre-orbital sequence (POS) television pictures approximately every hour; thus, Mars was viewed once each 15 degrees of planet rotation. This

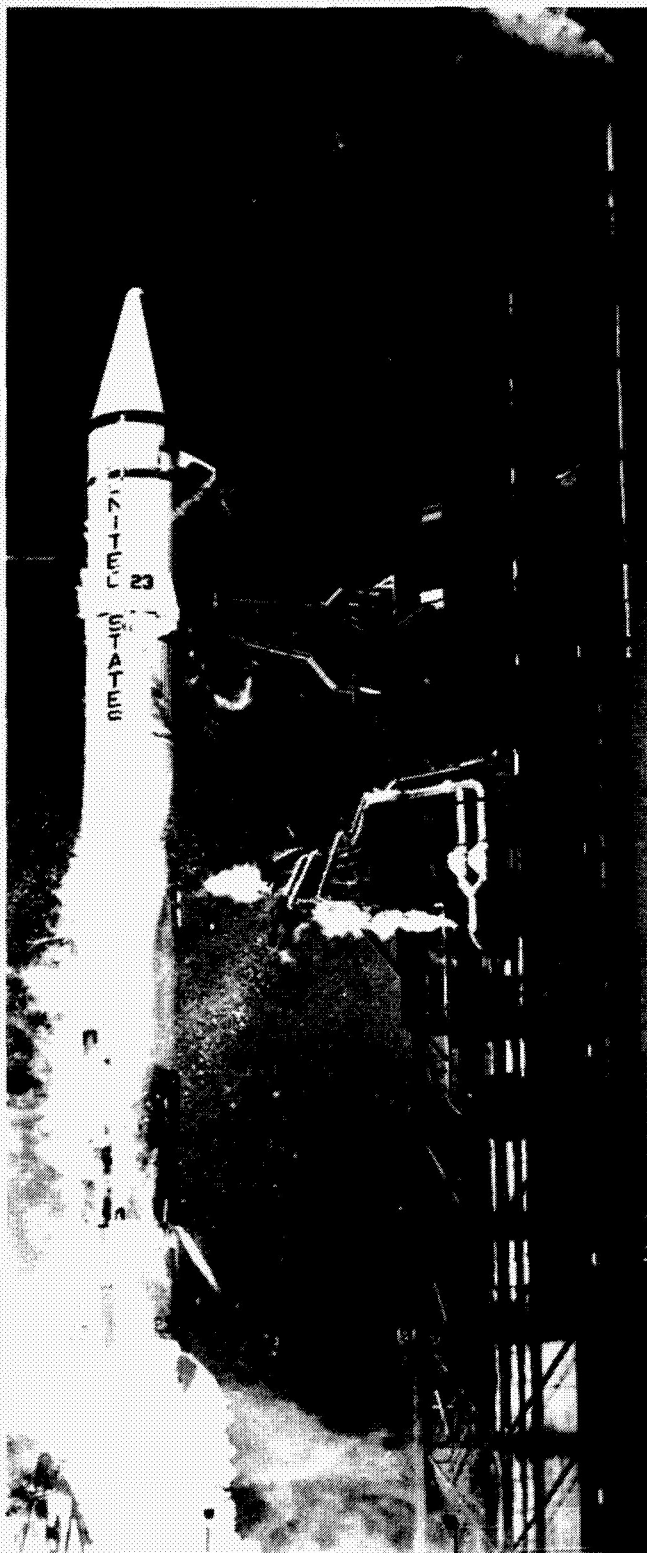


Fig. 1. Launch of the Mariner 9 spacecraft from Cape Kennedy by an Atlas-Centaur first-and second-stage launch vehicle, May 30, 1971.

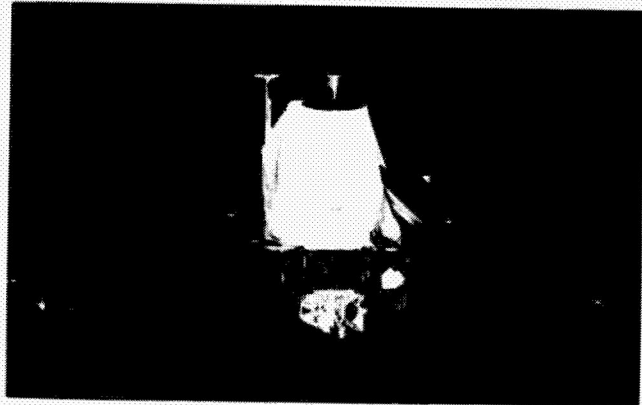


Fig. 2. The 2200-pound spacecraft is shown with the circular, green, high-gain antenna facing the viewer. The white shroud is a thermal blanket covering the propellant tanks of the 300-pound-thrust retro-engine. The rocket nozzle protrudes from the top with the low-gain antenna visible behind it. The scan platform carrying the scientific experiments is visible below the spacecraft. The Mariner 9 measures 7½ feet from the scan platform to the tip of the low-gain antenna and spans 22 feet, 7½ inches from tip to tip of the extended solar panels.

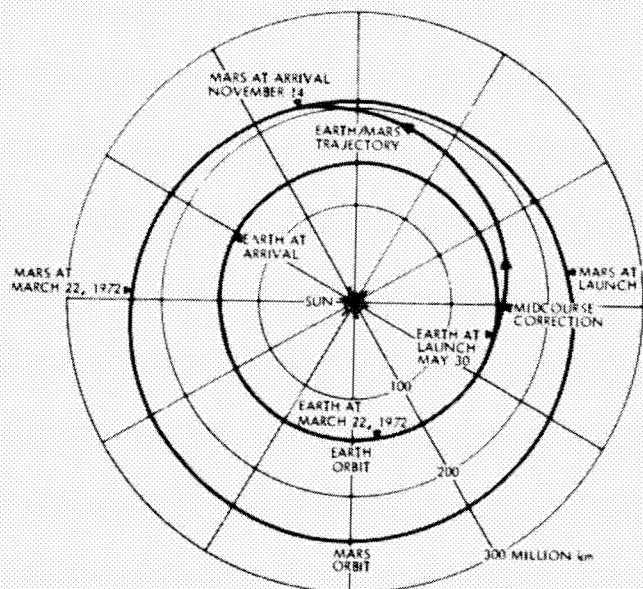


Fig. 3. The flight trajectory of the Mariner 9 is shown relative to the Earth's and Mars' orbital paths around the Sun. The positions of the planets at launch, at arrival, and at the end of the standard mission are indicated on the planet orbital track.

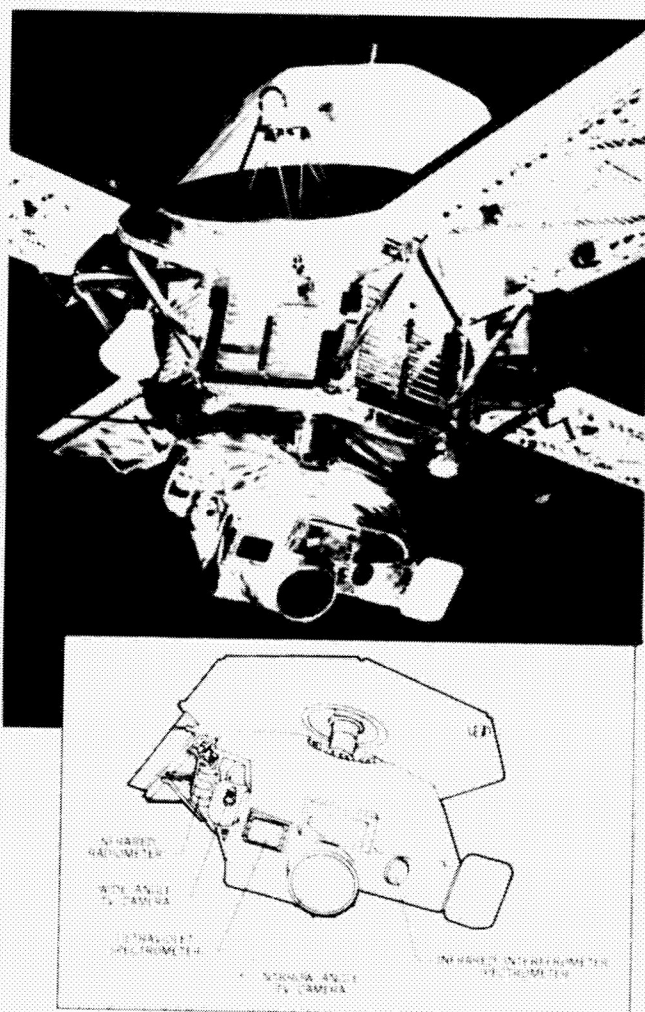


Fig. 4. Mariner 9's scientific instruments mounted on a movable scan platform. The television cameras were designed to "map" the surface of Mars; the spectrometers, to investigate the composition of the planet; and the radiometer, to determine the temperatures of the Martian surface and atmosphere.

series of pictures was followed by another series (POS 2) with similar timing. These pictures were taken as the spacecraft approached the planet to obtain a set of global, full-disk pictures to be used in low-resolution mapping. The last sequence (POS 3) was taken during a slightly shorter period than the others because of the insertion of Mariner 9 into orbit.

On November 14 GMT (November 13 PST), the spacecraft was inserted successfully into orbit around Mars (Fig. 5) by a 15-minute motor burn. (Figure 6 is a complete mission profile of Mariner 9 during its orbital operation phase.) Two days after insertion, on the fourth revolution around the planet, the spacecraft's orbit was corrected by a six-second firing of the rocket engine. However, because of a previously unknown variation in the gravity field of the planet's equatorial plane,

the average orbital period (11 hours, 58 minutes, 14 seconds) was found to be slightly too short, gradually changing the time relationship of the low point in the orbit (periapsis) to the tracking station (Fig. 7), a change which would eventually affect the reception of the data playbacks from the spacecraft.

At the time of Mariner's arrival, the planet-wide dust storm, which had been observed from Earth through telescopes starting in late September, was still obscuring the surface features of Mars. This storm actually was a bonus to scientists and ultimately provided many additional scientific findings; it was, however, responsible for the one and one-half month delay in the image-mapping phase of the mission, which could not be started until the dust storm subsided. During the waiting period, interim plans, subsequently designated Reconnaissance (Recon) I and II, were developed and implemented.

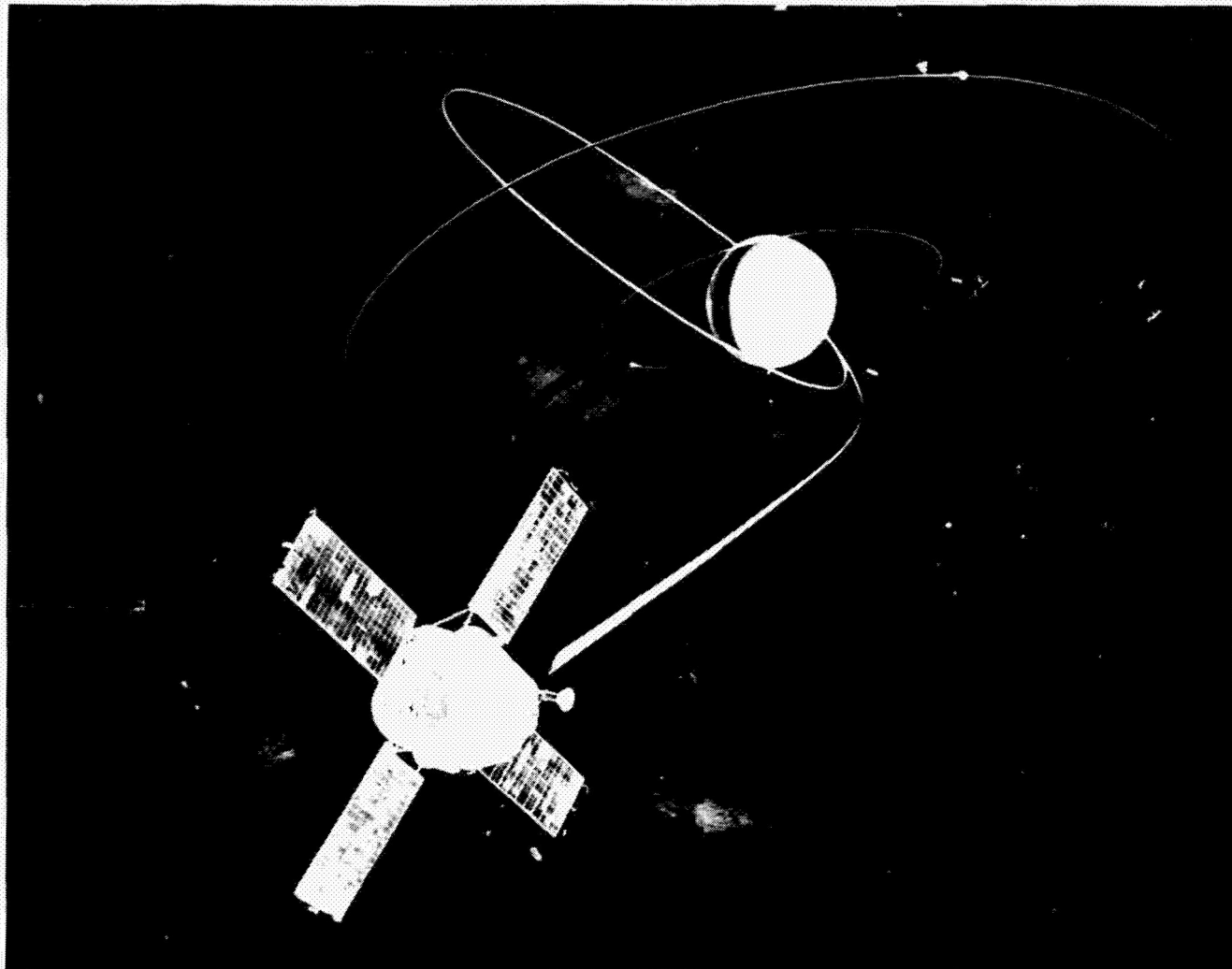


Fig. 5. Artist's concept of the Mariner 9 spacecraft as it approached Mars. The spacecraft turned from the sun position shown to point the rocket engine along the indicated flight path, then fire the engine to decelerate so that it could obtain the desired elliptical flight path around Mars. The orbits of the two moons, Phobos and Deimos, are in the equatorial plane of Mars. The 64-degree inclination of the spacecraft orbit made it possible to photograph the south and north polar regions of Mars.

Recon I, put into effect 12 days after Mariner 9 was inserted into orbit, supplied considerably more global information than planned. In particular, more data were supplied for the south polar regions than for mapping and variable features. Recon I was continued until 32 days after Mars orbit insertion, when Recon II was incorporated. This plan took maximum advantage of the fact that the spacecraft-Mars-Sun position was changing, providing different lighting angles and times in the orbital period when specific information could be gained. Spectral data from the dark side of the planet and ultraviolet limb-crossing data were included in both Recon I and II, and a constant effort was made to record as much data as possible.

The clearing of the dust storm became more apparent in mid-December, when dramatic changes were observed in the lower parts of the southern hemisphere between 60 and 90°S latitude. Clearing extended rapidly into the equatorial regions.

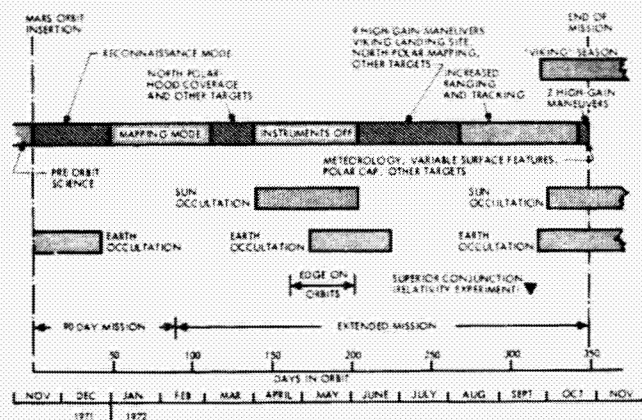


Fig. 6. Profile of the mission operation sequence of the Mariner 9 spacecraft.

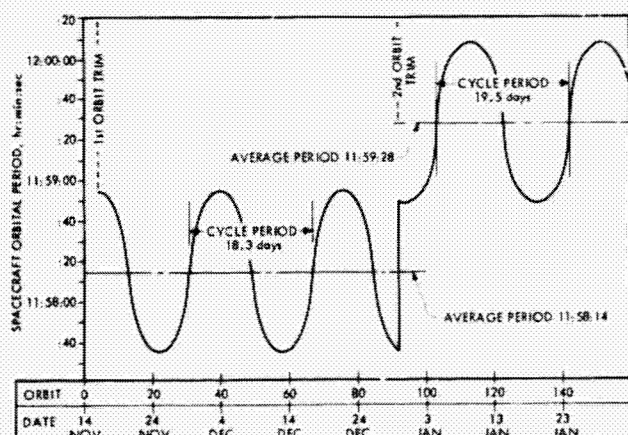


Fig. 7. Mariner 9 orbital-period variation after the first and second trim maneuvers. The Mars gravity difference with longitude caused the time for one spacecraft revolution to vary in this manner.

Preparations for the new mapping sequences were then put into effect.

A second trim maneuver was made on December 30, 47 days after Mars orbit insertion. This maneuver corrected the orbital period, coordinating the periapsis passage timing with the view period of the 64-meter (210-foot) antenna at the Goldstone tracking station in California (Fig. 8). The maneuver also changed the periapsis altitude from 1387 to 1650 kilometers (862 to 1025 miles), so that television coverage was broader and the mapping objective could be fulfilled in the time remaining for high data rate during the 90-day standard mission. This second trim was the last maneuver performed.

Mapping was performed in three 20-day cycles. The first cycle was designed to cover a latitude band from about 65 to about 20°S. The second cycle overlapped the areas from 30 to 20°S because the earlier pictures did not provide complete sidelapping coverage from orbit to orbit. Mapping in this cycle extended to about 20°N latitude. The third cycle completed any unrecorded areas in the 20 to 10°S latitude band and provided surface coverage from 20°N latitude to the polar hood at 45 to 60°N latitude, where surface detail was masked by atmospheric haze and clouds. At the end of the three cycles (February 29, 1972), after 110 days of orbital operations, all mission objectives had been fulfilled.

Operations continued daily through March 31, 1972. The distances between Earth and Mars were increasing, and the pointing direction of the high-gain antenna had moved off Earth. As expected, loss of telecommunications signal strength resulted in decreased data rates. Halfway through the third mapping cycle, the data rate had already been reduced from 16,200 to 8100 bits per second (Fig. 8). By the end of the third cycle, a combination rate of 8100 and 4050 bits per second was incorporated.

Picture sequences after the third cycle consisted primarily of special areas of interest (targets), with the selection of locations based on ultraviolet and infrared data as well as on television observations. One special data-taking sequence was acquired, when the spacecraft was maneuvered to point the high-gain antenna at Earth. The brief period of high-rate data during the high-gain antenna maneuver provided the last science coverage before the start of solar occultation (passage of the spacecraft through the planet's shadow). An engineering-test sequence was conducted with low data rates to confirm operational procedures after solar occultations.

Solar occultation began on April 2 and continued until June 4. Except for celestial mechanics and S-band radio occultation experiments, no science data could be acquired from the start of the spacecraft engineering tests before occultation until about June 8. On June 9, when another high-gain maneuver was made, scan-platform instrument data recorded on preceding orbits were played back to Earth.

This period of science data existed until the end of the mission on October 27, 1972. During the extended mission,

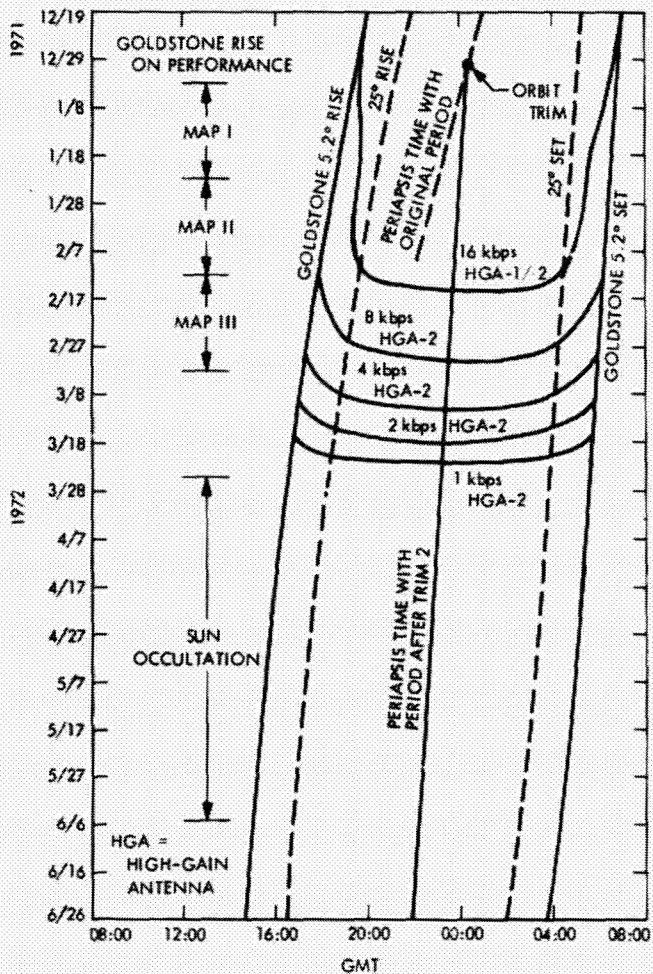


Fig. 8. Daily view period of the Deep Space Net (DSN) 64-m (210-foot) antenna, Station 14. The Mariner 9 second trim maneuver on revolution 94 changed the spacecraft periapsis and antenna zenith timing so that a favorable communication pattern could be maintained during the life of the mission.

11 playbacks yielded 329 television pictures as well as other scientific information. Most of the emphasis in June and July was placed on the north latitude and north polar cap surface mapping which, earlier in the mission, had been hidden by the north polar hood, the massive cloud formation over the pole during the winter season. Targets viewed earlier in the mission were subsequently re-reviewed to search for variable surface and atmospheric features or for higher-resolution images of geologic structures.

High-gain antenna maneuvers were not conducted from August 8 to October 12 because of requirements for the relativity test of the celestial mechanics experiment. Also, at about the time of superior conjunction on September 7, 1972 (Fig. 9) radio transmission was poor, thus making a high-gain antenna maneuver risky and the data return of questionable value.

A third period of Earth occultations began on September 27, 1972, providing an opportunity for the S-band radio occultation experiment to acquire additional occultation data at new points. On September 28, end-of-mission engineering tests were initiated for a better understanding of the condition and capabilities of the spacecraft at the end of its long and productive life. The seventh and last end-of-mission test was performed on October 17.

Mariner's life ended on October 27, when the supply of nitrogen gas, used for attitude stabilization, was depleted. On that date, Mariner 9 had operated for 516 days since its launch and for 349 days since its insertion into orbit. Mariner 9 will remain in orbit for a minimum of 50 years before it crashes on the surface of Mars.

The spacecraft has transmitted 54 billion bits of science data, including more than 7300 television pictures of Mars and its two natural satellites, Phobos and Deimos, and has mapped 100 percent of the surface of Mars — an excellent performance by the first man-made satellite ever to orbit another planet.

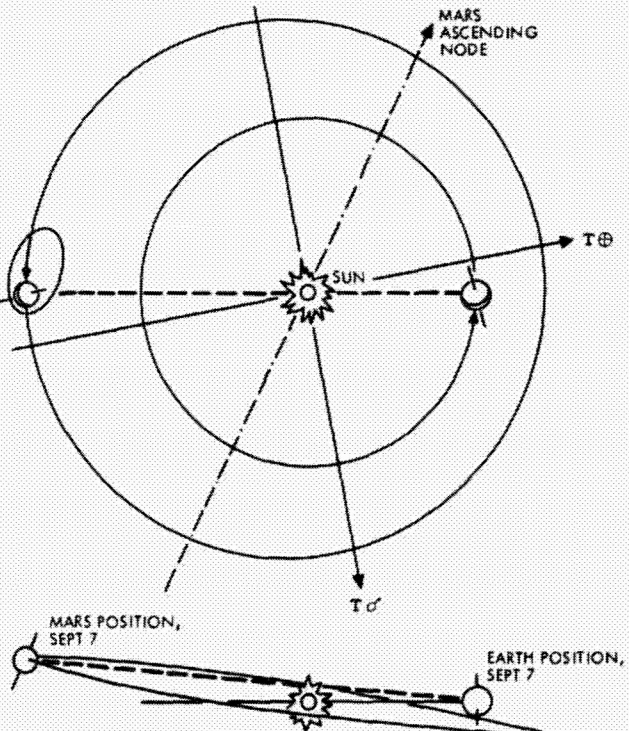


Fig. 9. Mariner 9 superior conjunction, September 7, 1972. Planet orbit geometry causes line of sight of flight path to pass less than one degree above the north limb of the sun.

Surface Maps

One of the primary objectives of the Mariner 9 mission was to photographically map the planet, Mars, by taking wide-angle pictures which would establish the positions of surface features and form the geodetic grid. Pictures of higher resolution were to be taken as the spacecraft approached the planet to provide contiguous coverage of the surface. However, because of the raging atmospheric dust storm (Fig. 10), these pictures could not be taken.

Although the dust storm prevented the recording of these pictures, significant data defining the shape of the planet were derived during the early part of the mission from occultation points (Fig. 11) by the S-band occultation experiment. As the

spacecraft approached the solid disk of the planet, the radio signals were altered by propagation waves through the planet's atmosphere. The radio signals passed through the upper, then the lower, atmosphere. During this time, variations could be detected in the radio transmission characteristics. When the trajectory carried the spacecraft completely behind Mars, out of view of Earth (Fig. 12), all radio signals were blocked by the solid surface and communications were cut off, providing an accurate measure of the shape (radius) of the planet. Conversely, while the spacecraft was emerging from behind the solid disk at another point of the planet, its shape, the lower, then the upper atmosphere was measured.

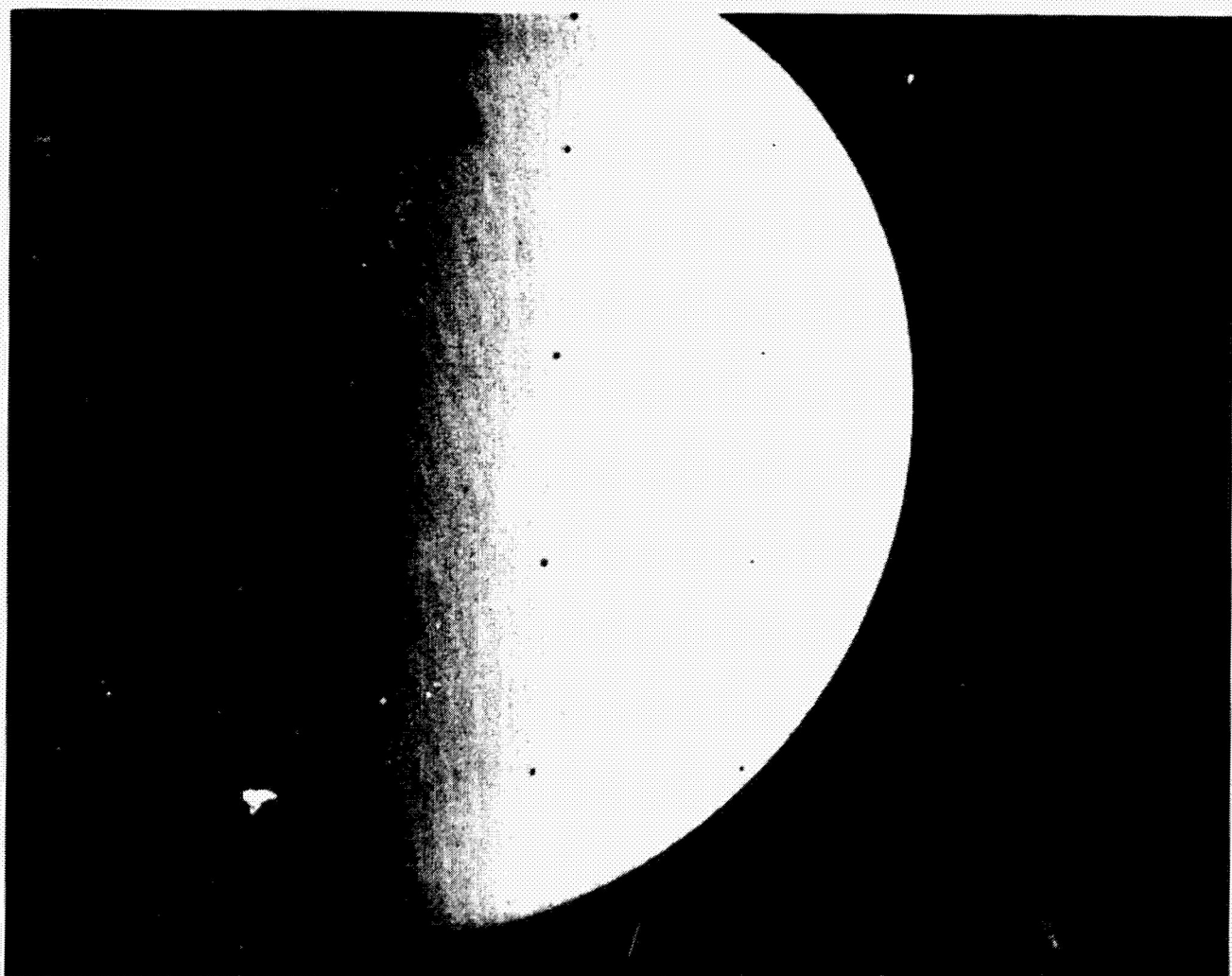


Fig. 10. Preorbital picture of Mars showing the only features which could be seen through the global dust storm: the four dark spots just north of the equator and the light patch of the residual south polar cap.

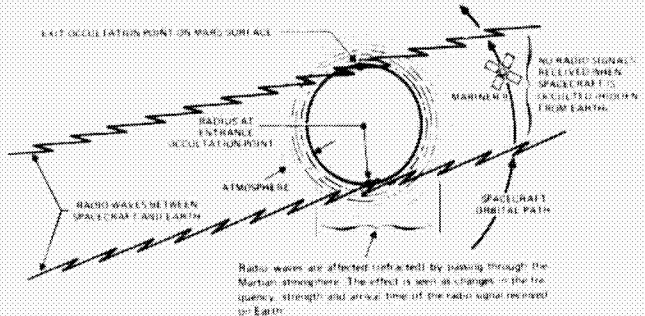


Fig. 12. The Mariner 9 S-band occultation experiment was performed by using the radio communication system of the spacecraft and the DSN facilities on Earth to measure the refraction of the radio beam by the Martian atmosphere and the precise time of spacecraft occultation. Mariner 4, 6, and 7, because they flew by Mars, obtained only two occultation points each, one entry and one exit point. Mariner 9 obtained over 200 occultation points as it circled Mars. At each point, calculations provided information about the density of charged particles in the ionosphere of Mars; the temperature, pressure, and density in the lower atmosphere of the planet; and accurate measurements of the radius of Mars.

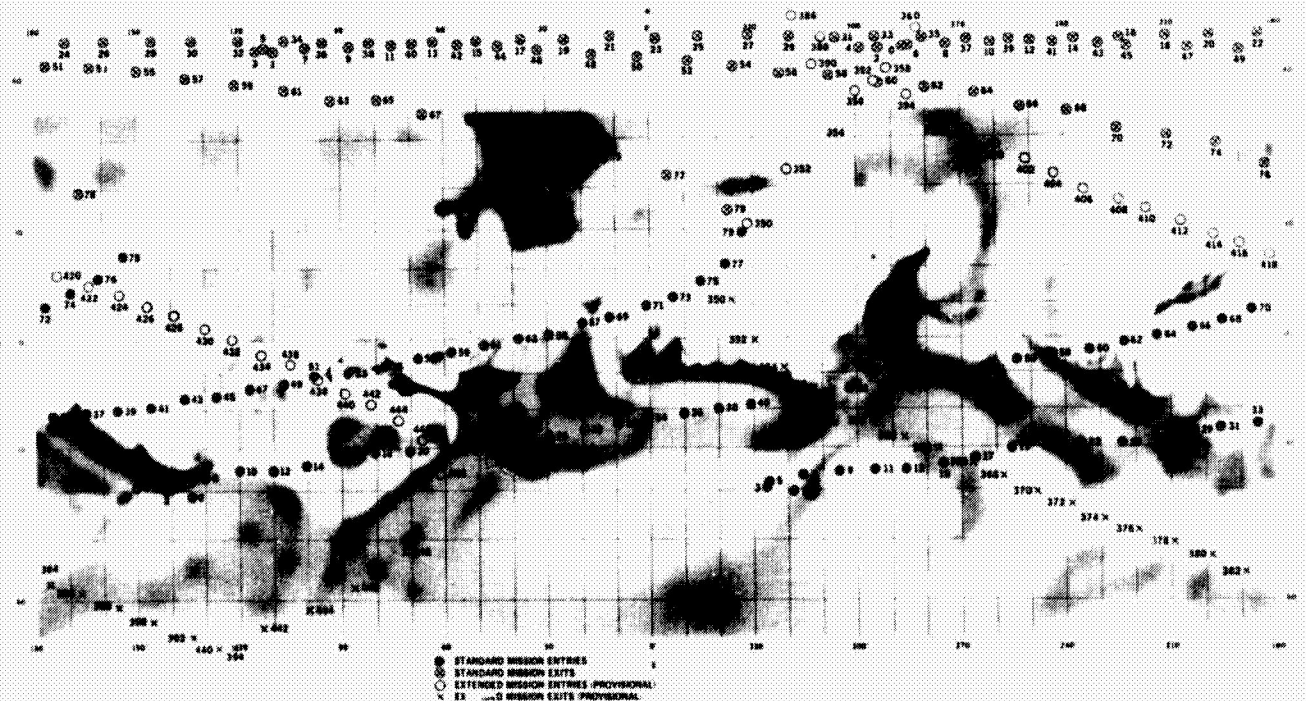


Fig. 11. Mercator map showing the locations on the Martian surface of the occultation points obtained during the S-band occultation experiment. The numbers indicate the revolution during which the occultation occurred. The circles, both filled in (●) and open (○), show the entrance points; and the "X"s, both circled and uncircled, indicate the exits. An accurate measurement of the radius of the planet was obtained at each of these points.

Two occultations occurred each day during this first phase of the mission, for a total of 79 occultations. Each one provided two specific measurements totaling 158 measurements of the planet's radius. Later in the mission, more occultation points were accumulated. The information gained in the first part of the mission was used during the operational period to

analyze the Martian surface for a better understanding of the previously unknown planet. Surface elevation differences varied more than 14 kilometers (9 miles) from the low points to the high points. Variations in the topography of Mars (Fig. 13) are more extreme than in the topography of Earth, a planet twice the diameter of Mars.

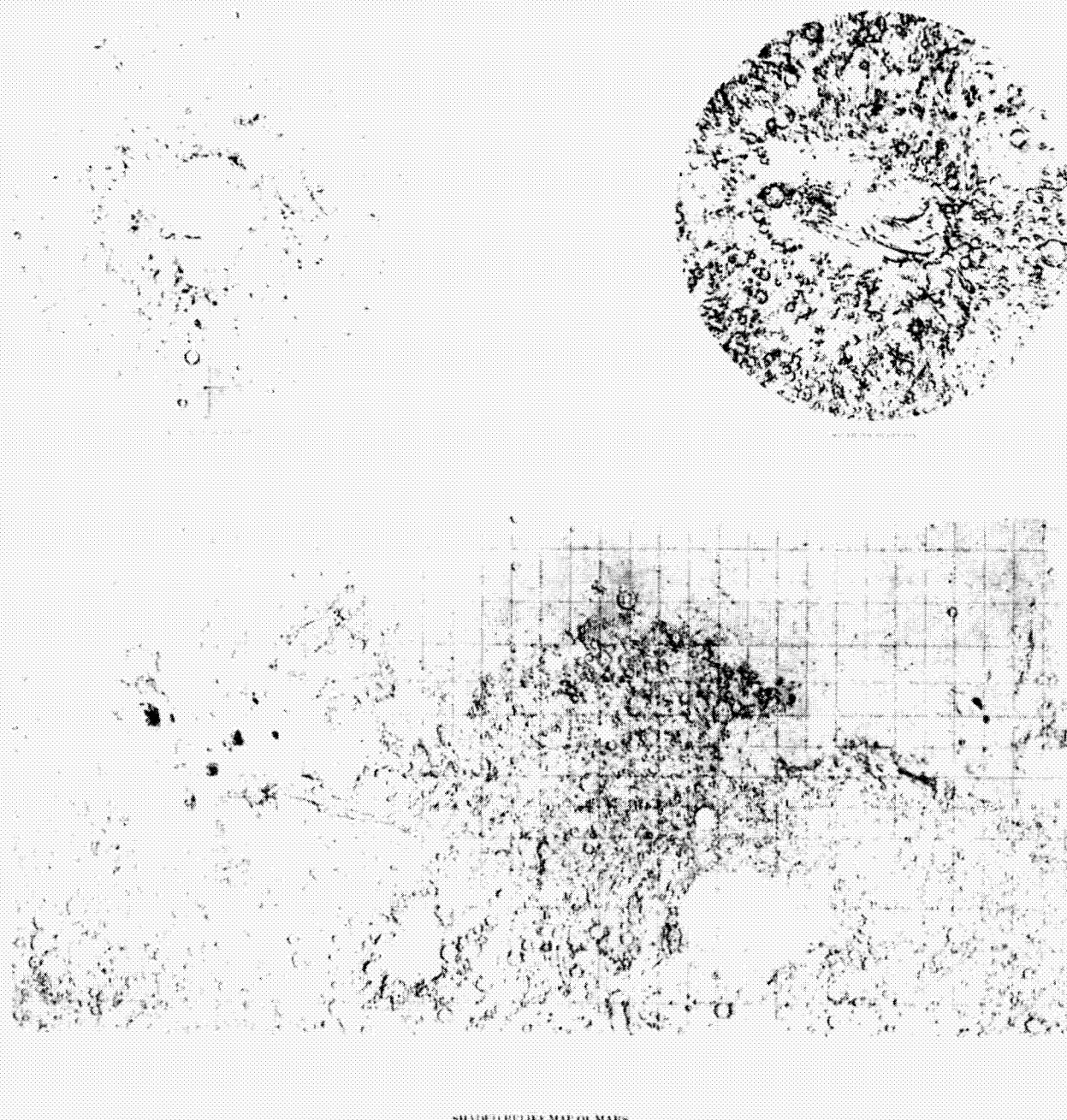


Fig. 13. Shaded relief map of Mars showing the entire surface of the planet with the polar caps at their minimum size. in this air-brushed rendition, the light and dark or color markings do not show; the physical features appear as they would if lighting conditions were the same at all parts of the planet. (Scale, 1:25 million; produced by the U.S. Geological Survey, Flagstaff, Arizona)

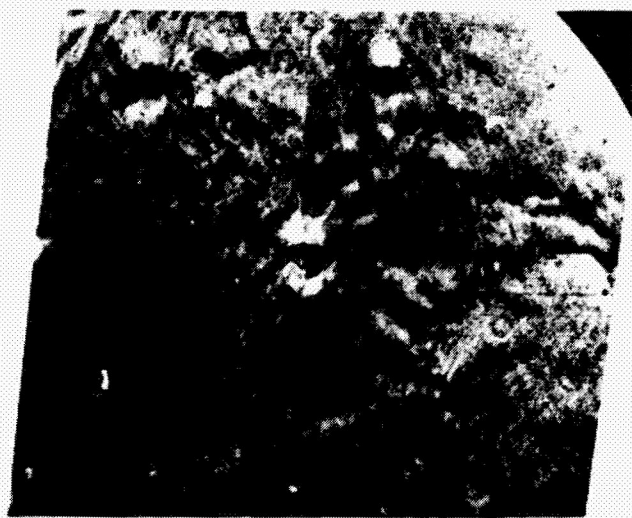
Surface Characteristics

The pictures taken in the three pre-orbital science sequences gave total global coverage of the dust-covered planet on which only five distinct features were visible: the south polar cap and four dark spots (Fig. 14). Toward the end of December, when the dust storm cleared and the surface characteristics could be clearly observed, these four spots were revealed as volcanic mountains on the face of Mars (Figs. 15 through 18). One feature, known as Nix Olympica, is the largest volcanic formation ever seen by man. The diameter of the volcanic shield is greater than 500 kilometers (310 miles); the height from the surrounding plains to the highest point on the lip of the caldera is 24 kilometers (about 80,000 feet), almost three times the height and twice the diameter of the island of Hawaii (the largest similar type of feature on Earth). The other spots, provisionally labeled North Spot, Middle Spot, and South Spot, are not as large individually. However, combined with the 6-to 8-kilometer (4-to 6-mile) height of the Tharsis Ridge on which they are located, they rise to elevations very close to that of Nix Olympica, and their base diameters are about 300 kilometers (200 miles).

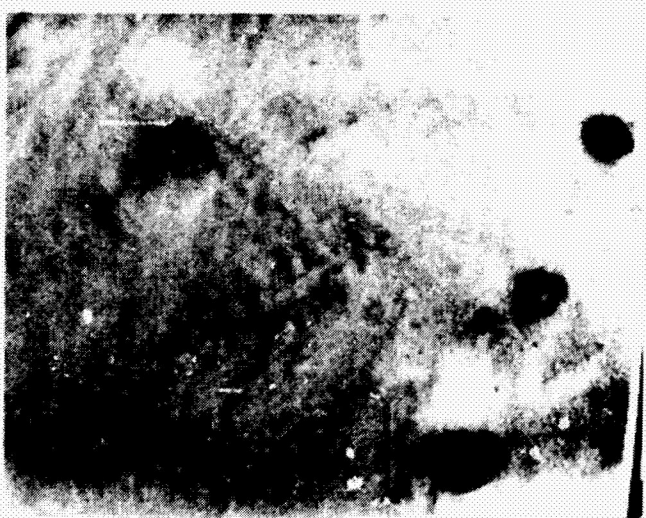
The boundaries of the south polar ice cap, compared to those photographed by Mariner 7, held amazingly constant during the summer period (Figs. 19 and 20). The permanently capped areas are apparently smooth and flat with a water-ice



Fig. 15. The dark spot, Nix Olympica, seen through the dusty atmosphere, looks like a volcanic crater. The many terraces and the cusp of the outer perimeter indicates that the 60-kilometer (40-mile) feature has experienced many epochs. The light lines across the picture result from the computer-enhancement process acting on the black reseau marks which are part of the picture data.



(a)



(b)

Fig. 14. The four dark spots seen through the dust storm. (a) A four-picture mosaic of computer-enhanced photographs which not only show the four spots but also reveal many details of features of the dust-laden atmosphere which could not be seen without enhancement. The spot to the left is in an area previously known as Nix Olympica (Snows of Olympus). The three spots to the right, in the general region known as Tharsis, were named North, Middle, and South Spot, respectively. An atmospheric wave can be seen extending southwest from South Spot for a distance of more than 1000 kilometers (620 miles). (b) A single picture, computer-enhanced, shows the crater-like nature of the dark spots.



Fig. 16. North Spot (Ascreus Lacus). Oblique view of the crater complex near Ascreus Lacus in the Tharsis region of Mars taken by Mariner 9. This complex is the northernmost of the prominent dark spots observed by Mariner during its approach to the planet. The spot consists of several intersecting, shallow, crater-like depressions. The main crater complex is approximately 21 kilometers (13 miles) across. The crater was visible through the dust storm because it is in a relatively high area. The faint circular markings outside the crater are believed to be atmospheric features.

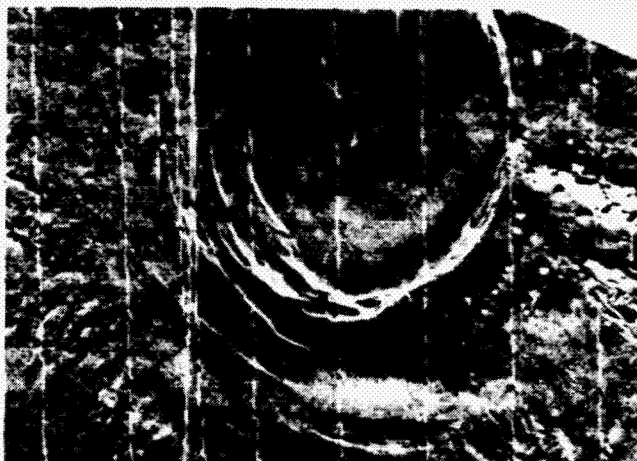
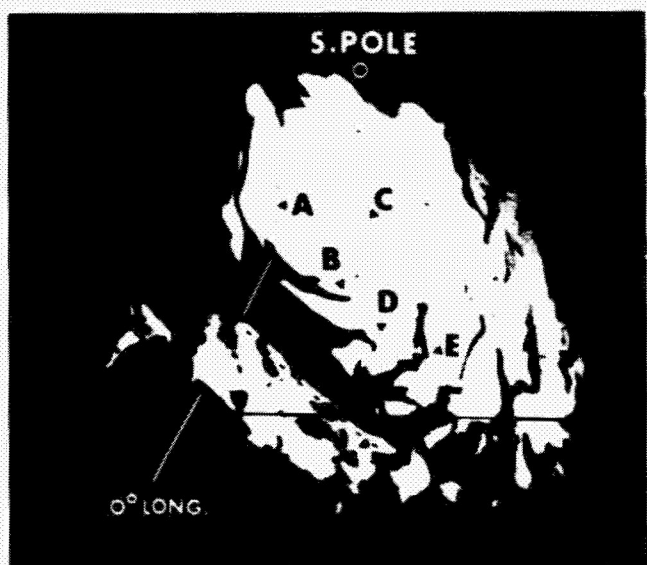


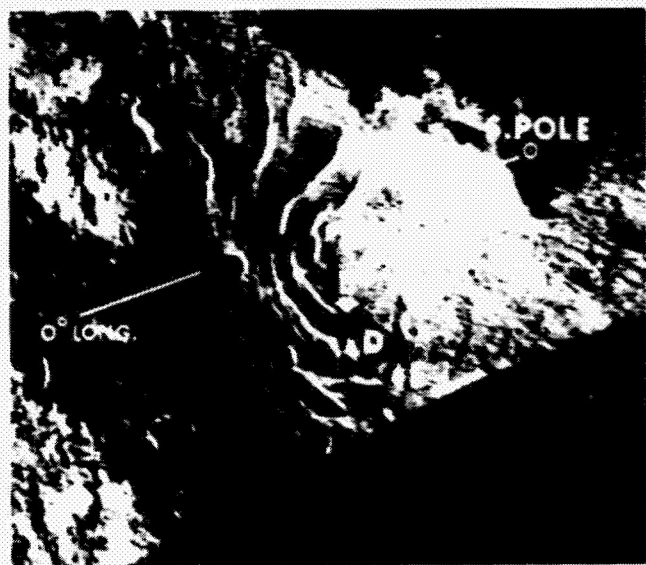
Fig. 18. South Spot. This Martian crater, 115 kilometers (70 miles) in diameter, is near Nodus Gordii (the Gordian Knot). South Spot was photographed on November 28, 1971. The crater and its immediate surroundings are high ground, emerging island-like from a sea of wind-blown dust. In pictures taken 48 hours later, the edge of the dust cloud had shifted, obscuring the ridges and valleys on the outer northwest rim. The multiple concentric fractures on the western rim and the abundant rimless craterlets suggest that this is a crater or caldera. South Spot is the largest caldera even seen by man.



Fig. 17. Middle Spot. A volcanic crater 65 kilometers (43 miles) wide, is located a few degrees north of the equator near Pavonis Lacus. Detail of the surrounding terrain was obscured by atmospheric dust.

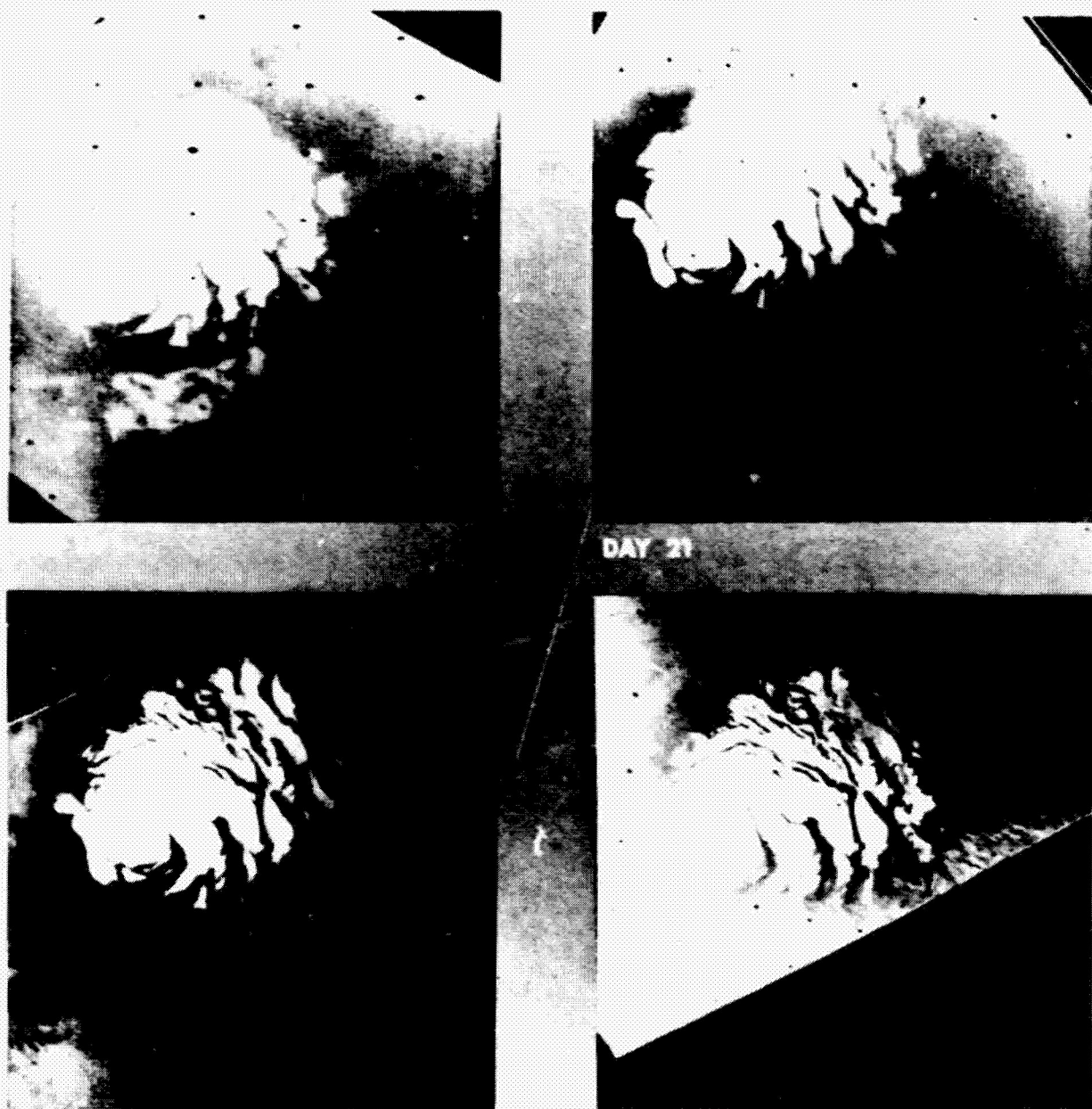


(a)



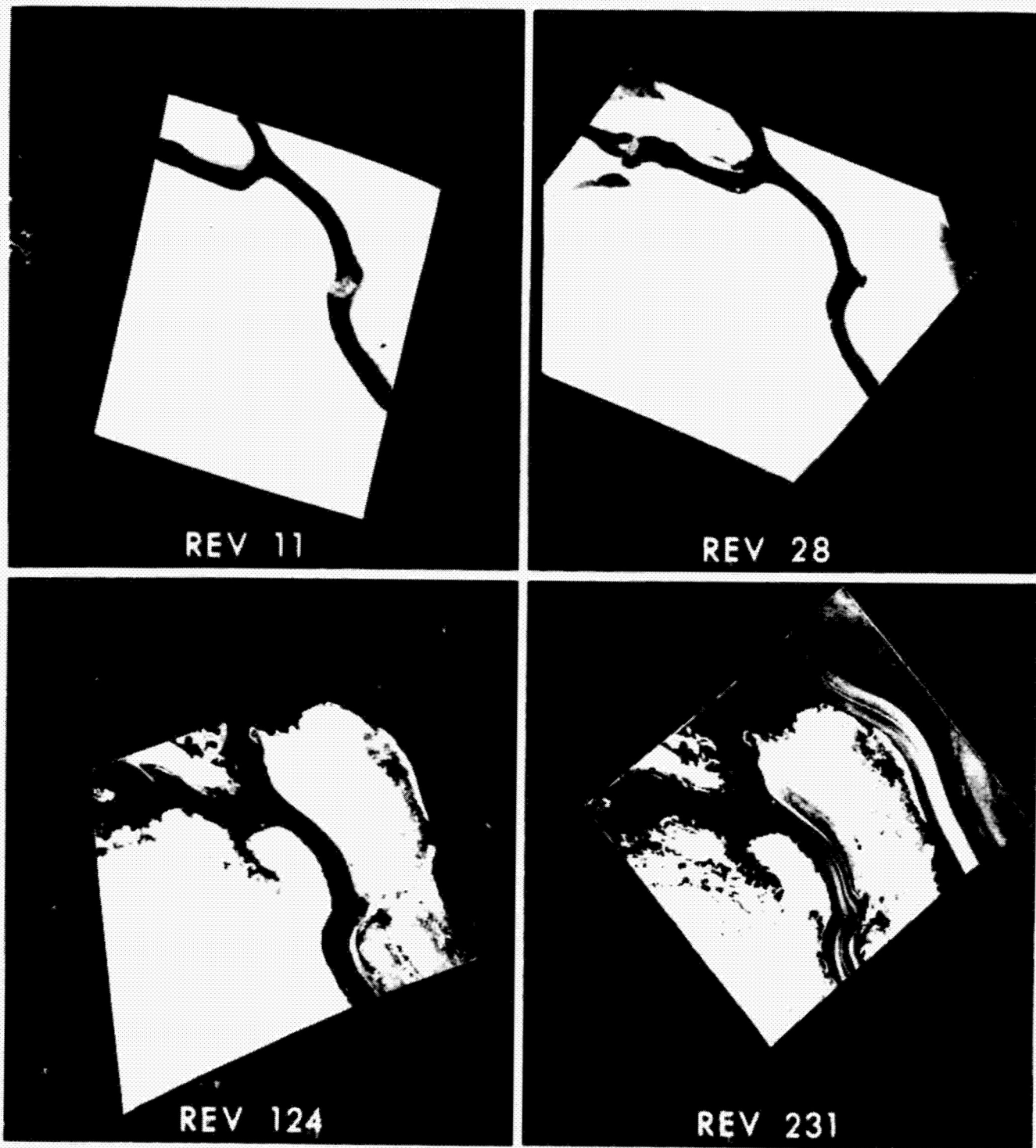
(b)

Fig. 19. Views of the south polar cap: (a) Mariner 9, (b) Mariner 7. The dark marking in the Mariner 9 wide-angle picture of the cap is correlated with the light markings on a narrow-angle picture from Mariner 7. The Mariner 7 image has been rectified and computer-enhanced. Although this version shows strong contrast, the entire area actually was covered by frost.



(a)

Fig. 20(a). Boundaries of the south polar cap during the summer season showing residual cap evolution. The four wide angle photographs have been computer-enhanced, rectified, and scaled to permit visual comparison. Significant change can be seen in cap boundaries in the top two photographs, but relatively stable conditions for the remaining summer season are shown in the lower. The earlier photographs are somewhat obscured by the dusty atmosphere. The residual cap dimension is about 300 by 350 kilometers (200 by 230 miles).



(b)

Fig. 20(b). "The Fork", the dark channel seen lower left in the preceding wide-angle photographs, is shown in four narrow-angle pictures taken at different times throughout the mission. The three photographs obtained on revolutions 11, 28, and 124, respectively, were taken with sun elevations 15 to 20 degrees above the horizon. The fourth picture, taken with a sun elevation of about 4 degrees, vividly displays the topography of the sinuous slopes.



(a)



(b)

Fig. 21. Laminated terrain, an unique layered formation in the south polar region. (a) Edge of laminated surface borders on an eroded formation called "etch pits". (b) Laminated surface with patches of residual cap showing.

surface rather than the carbon-dioxide ice of the large early spring cap. The edges of the residual cap boundaries showed greater slopes than the frost-covered areas which remained during the "hot" summer period. The exposed terrain appeared layered (Fig. 21) and quite different from anything on Earth. The terrain may be composed of substantial amounts of water-ice overlaid with soil or dust, possibly carried there by dust storms similar to the giant storm of 1971 and built up over many millions of years. The only other cap markings are areas that seem to be grooved in radial or slightly spiraled patterns

similar to the type of grooving seen in glacial formations on Earth (Fig. 22). The bulk of the terrain in the southern hemisphere is saturated with impact craters, resembling the crater-pocked terrain observed on the lunar surface. This type of terrain, viewed by Mariner 4 in 1965 and by Mariners 6 and 7 in 1969 (Figs. 23 and 24), first led scientists to believe that Mars was Moon-like.

Between the heavily cratered terrain and the polar glacial area are terrain features called "etch pits" (Figs. 25 and 26). These etch pits may be caused by wind erosion or by warming cycles in which deposits of permafrost have melted away. The formations have no lunar or terrestrial counterparts, and thus are unique to Mars.



Fig. 22. Laminated terrain. There are many layering marks where slopes are steepest. The flat surfaces are grooved. The grooves are reminiscent of wind erosion of earthly glacial formations.



Fig. 23. A mosaic of wide-angle photographs taken by Mariner 6 in July 1969 shows more than 1500 kilometers of heavily cratered surface in the mid-south latitudes. Even the narrow-angle pictures of the white-bordered areas show the small craters in the high-resolution surface detail. Lack of geological variation in photographs taken during the 1965 and 1967 flyby missions gave a mistaken impression of Martian geology.

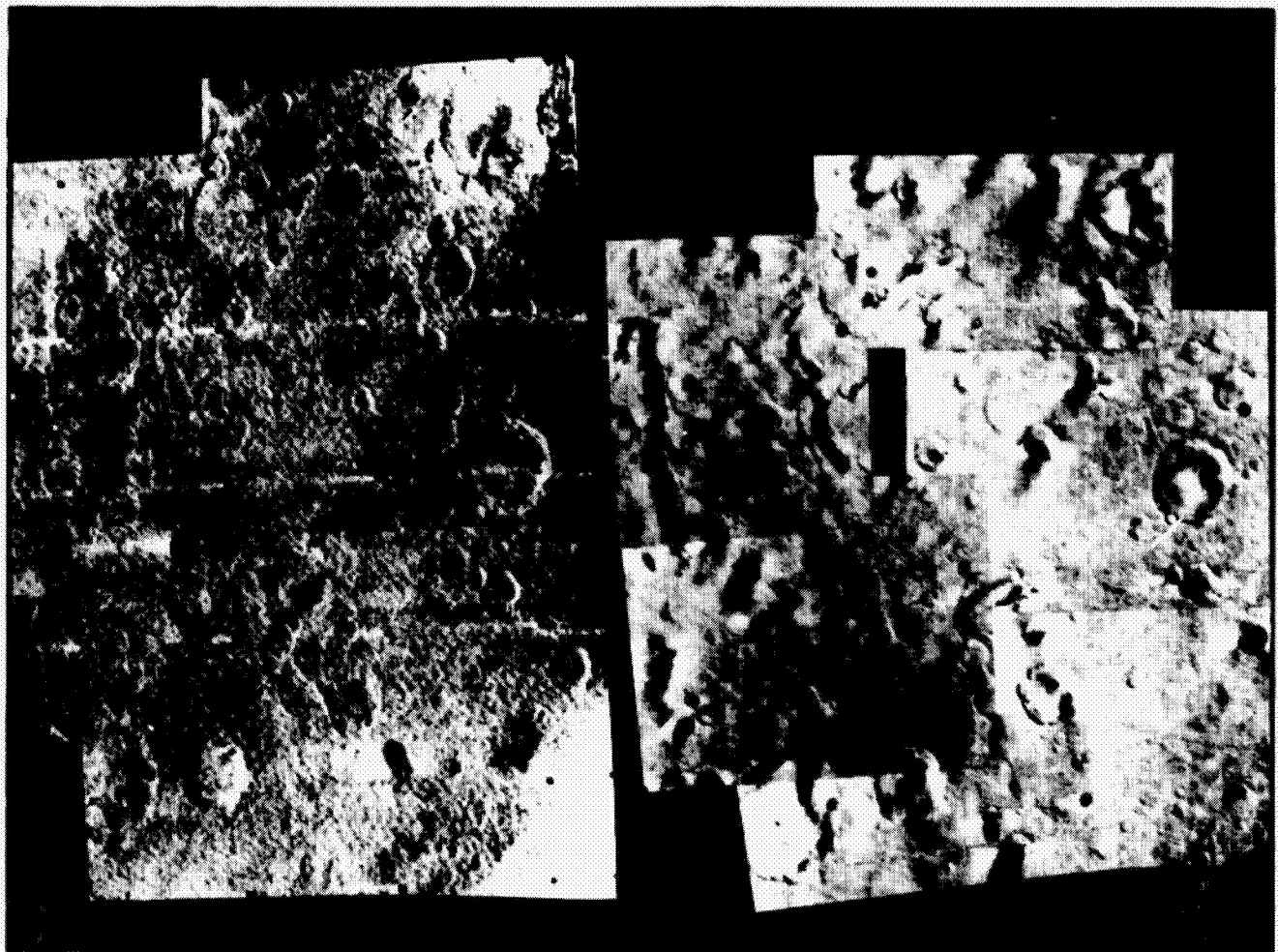
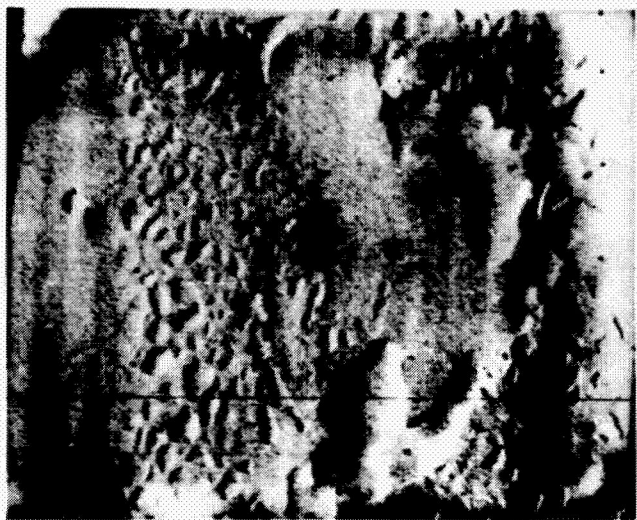


Fig. 24. Comparison of an area in the southern hemisphere photographed by Mariner 7 in Martian early spring, August 1969 (left) with the same area photographed by Mariner 9 in Martian midsummer, January 1972. The surface features can be readily identified in both photographs, but the albedo, or shading, has changed. The difference in the surface appearance is probably caused by dust deposited by the global dust storm. If winds throughout the remainder of the Martian year blow the dust away, the surface seen in early spring would again be exposed.



(a)



(b)

Fig. 25. Extraordinary pits and hollows photographed about 800 kilometers (500 miles) from the south pole on revolution 108. These features give rise to some provocative questions about the geological processes which have shaped the landforms of the polar region. (a) The two large closed basins are about 16 kilometers (10 miles) across. Unlike collapse features resulting from volcanic withdrawal, these hollows exhibit no interior terraces. Conceivably, these structures may have resulted from the thawing of large accumulations of ground ice. Another possibility is that they are deflation hollows developed by wind action in loosely consolidated materials. (b) Contrasting terrains of Novus Mons area (66°S and 325°W) are seen in the composite of two high-resolution pictures. The smooth but finely striated area in the center stands at a higher elevation than the more irregular terrain in the top of the picture. This smooth feature is about 70 kilometers (43 miles) across. At the bottom, albedo patterns, which are more pronounced, conceal the relief patterns.



Fig. 26. A pattern of a complex of transecting ridges 2 to 5 kilometers apart. The ridges are probably composed of a resistant material, which filled crosscutting fractures and then later became exposed when erosion removed the surrounding weaker material. The resistant material may have been molten rocks intruded into faults or dust blown into crevasses in an ancient ice mass. The area shown is approximately 42 by 48 kilometers (25 by 30 miles).

The region of the northern hemisphere, apparently flooded with lava flows, has an entirely different and unexpected appearance. The area near the four volcanic mountains show signs of later stress by crustal movements (Figs. 27 and 28). In one example, fracturing occurs in three major directions, with uplifts and tilted blocks. Farther to the east lies a lattice of canyons (Fig. 29) with more extensive fracturing and a more rugged appearance than Earth's Grand Canyon. This canyon complex, however, is overshadowed by a giant rift zone (Fig. 30), extending some 4000 kilometers (2500 miles) farther east across the face of Mars. This feature, as deep as 6 kilometers (4 miles) and as wide as 125 kilometers (75 miles), outstrips the great rift zone in Eastern Africa. Other areas nearby, called "chaotic terrain" (Fig. 31), a jumbled type of surface produced by slumping, seem to have no terrestrial counterpart. To the north is an expanse, similar in appearance to the lunar mare areas, which extends around the entire longitude of the planet. This entire area has been flooded with basalt (Fig. 32). Its smooth appearance is an indication that the flooding occurred after the planet experienced an era billions of years ago in which impacting meteorites left it completely saturated with impact craters.

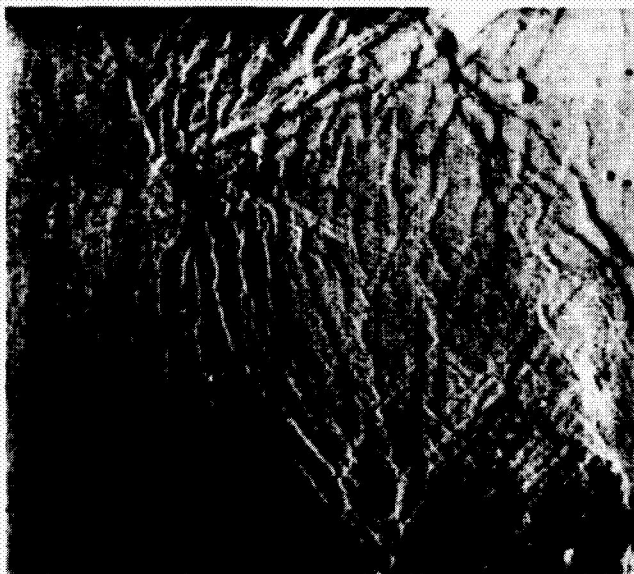


Fig. 27. Striking wide-angle view of the surface in the area of Phoenicis Lacus, taken during the spacecraft's 67th orbit. This plateau lies about 6 kilometers (3-1/2 miles) above the mean elevation on Mars. The few craters indicate that the surface is a volcanic deposit from a relatively young lava flow, which was later broken by faults that cut the rocks into mosaic-like fragments. The fault valleys are more than 2 kilometers (1-1/2 miles) across. This picture was taken from an altitude of 6500 kilometers (4,000 miles) on December 17. North is at the top. The center of the picture is 17.5 °S latitude and 110 °W longitude.

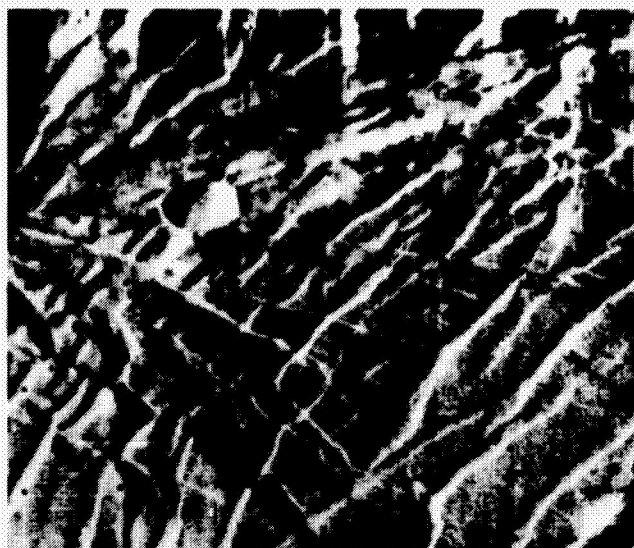


Fig. 28. This narrow-angle photograph shows details of the complicated faults in the center of Fig. 27. Uplifted and tilted blocks are identifiable.



Fig. 29. An intricate network of mighty canyons appears to hang like a giant chandelier from the Martian equator in a picture taken January 10, 1972. This picture, which covers an area 540 kilometers wide by 420 kilometers high (330 by 260 miles), provides dramatic evidence of erosional processes at work on the fractured volcanic tablelands of Noctis Lacus. Sunlight is coming from the east (right side) of the picture.

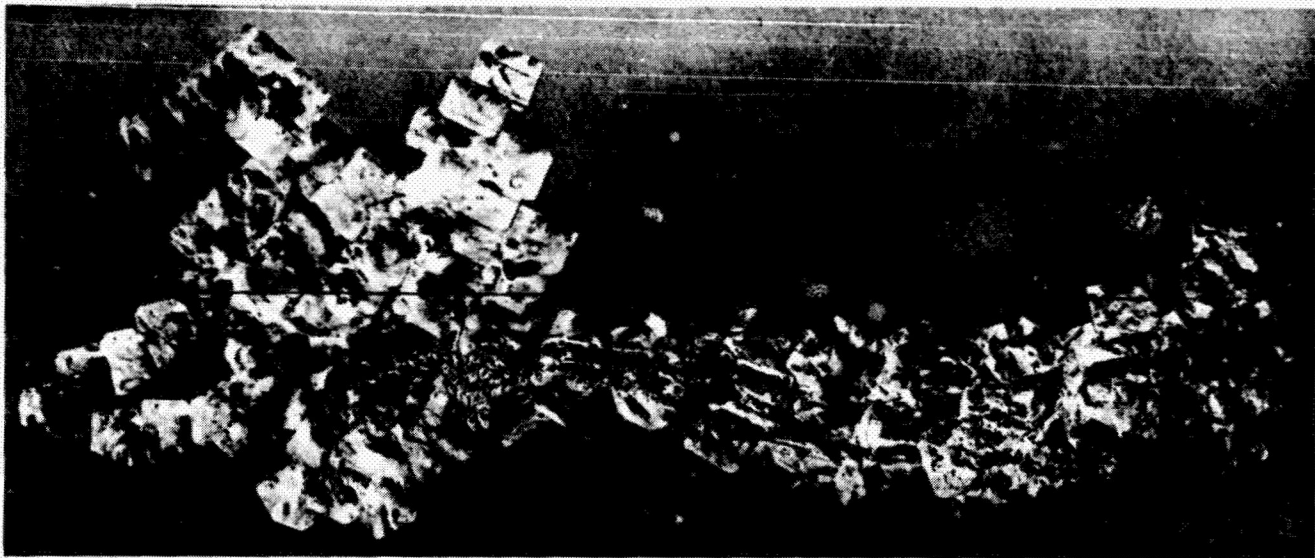


Fig. 30. More than 100 photographs were used to complete this mosaic of the equatorial region showing the four volcanic mountains on the left and the canyon lands and giant rift to the right. Some of the highest and lowest elevations on Mars are located in this relatively small part of the planet.



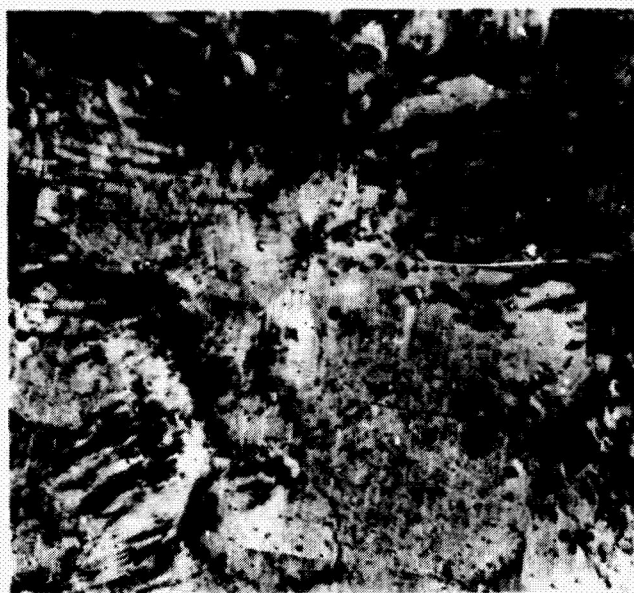
Fig. 31. (a) Wide-angle photograph of extremely irregular, jumbled terrain north of Coprates Canyon. This hummocky area, apparently caused by a landslide from the high, smoother terrain, is similar to the chaotic terrain seen in photographs taken by Mariner 6 in 1969. (b) A high-resolution photograph of the area shown to the lower right of center in the wide-angle picture. The low sun angle enhanced the topographic detail, showing the slumping and breaking of the terrain by the sliding action.



Fig. 32. The northern hemisphere of Mars from the polar cap to a few degrees south of the equator, taken August 7, 1972. Complex sedimentary systems can be seen in the area of the north polar ice cap, which was shrinking in the late Martian spring. Fractured terrain, partially flooded by volcanic extrusions, is visible in the center of the disk. The volcanic mountains can be seen at the lower left and the west end of the great equatorial canyon, Coprates, at lower right. The three computer-enhanced photographs comprising the mosaic were taken 84 seconds apart from an average range of 13,000 kilometers (8500 miles).



(a)



(b)

Fig. 33. Wide-angle camera views of albedo surface features. (a) Enlarging dark features were observed during the mission in this area of the southern hemisphere (70°S , 259°W). (b) Streaking seen in part of the classical feature in the northern hemisphere known as Syrtis Major (13°N , 283°W) is indicative of strong surface winds.

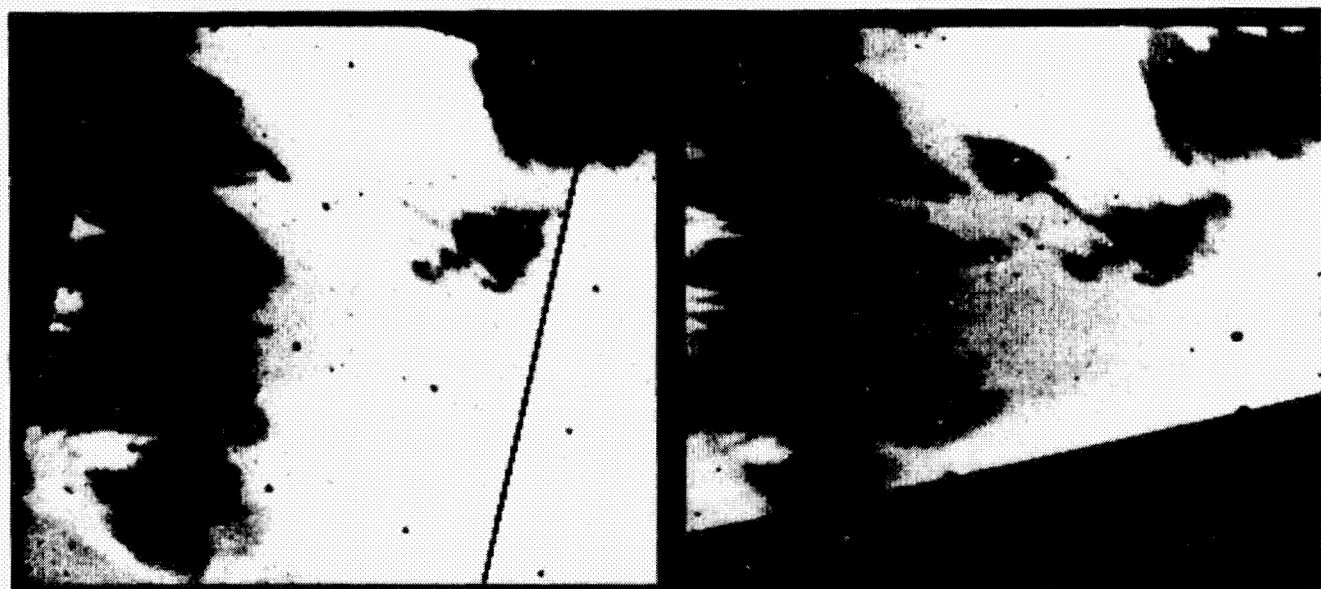
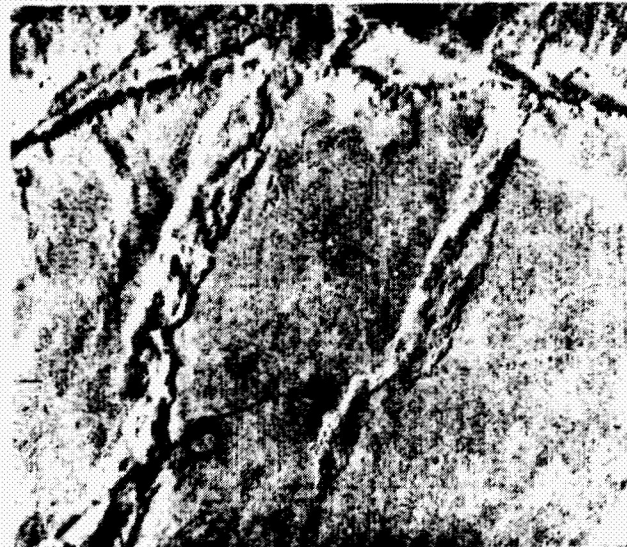
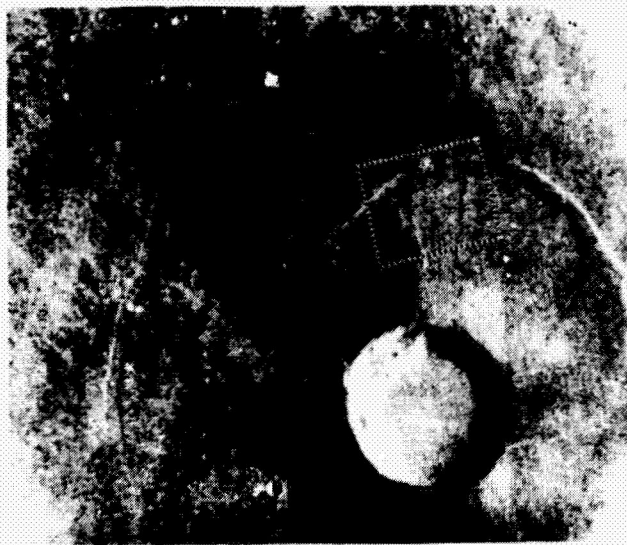


Fig. 34. Two narrow-angle photographs of the area seen in the center right section of Fig. 33(a) show a leaf-like, dark feature. This 8-kilometer (5-mile) feature developed between the recording of the left photograph on orbit 99 and the right photograph on orbit 126, thirteen days later. The total area shown is approximately 45 kilometers (28 miles) wide.

Variable surface changes detected throughout the mission indicate that areas light in color are fine, particulate matter (Fig. 33), mobile in the winds. The dark areas are coarser, granular material or rocks and are less mobile, or possibly completely immobile, in the winds. In all cases in which

surface changes were observed, the boundaries of adjacent light and dark material changed so that the light area always retreated or showed a change, and the expanse of the dark area enlarged (Figs. 34 and 35). A somewhat uniform dust layer may be deposited over the surface of the planet by global dust storms and then, later, moved about by local dust storms, exposing the darker surface material. In some regions, the dark areas in the floors of craters (Fig. 36) showed a pattern similar to sand dune fields on Earth, indicating a larger granularity than lighter colored dust.

The surface characteristics and composition of the varied types of terrain have been compiled to determine the stratigraphy of Mars (Fig. 37). The older crater areas appear modified by processes of tectonics, volcanism, glaciation, and wind and water erosion.



(a)



(b)

Fig. 35(a). Wide-angle view of the volcanic crater, Middle Spot, 40 kilometers (25 miles) wide, located near Pavonis Lacus on the equator of Mars. A narrow-angle picture of the north flank (white rectangle) shows ridges, which appear similar to lunar mare ridges inferred to be breaks in the crust, along which extrusions of lava have taken place. The photograph were taken on December 16 and 22, 1971, when obscuration by the dust storm was subsiding in the higher elevations. (b) A narrow-angle photograph of the same area taken March 1972, showing the development of two dark areas. It is calculated that, because of the high altitude and low atmospheric density, the winds had to be greater than 500 kilometers (300 miles) per hour to clear the dust from the surface to expose the dark underlying material.

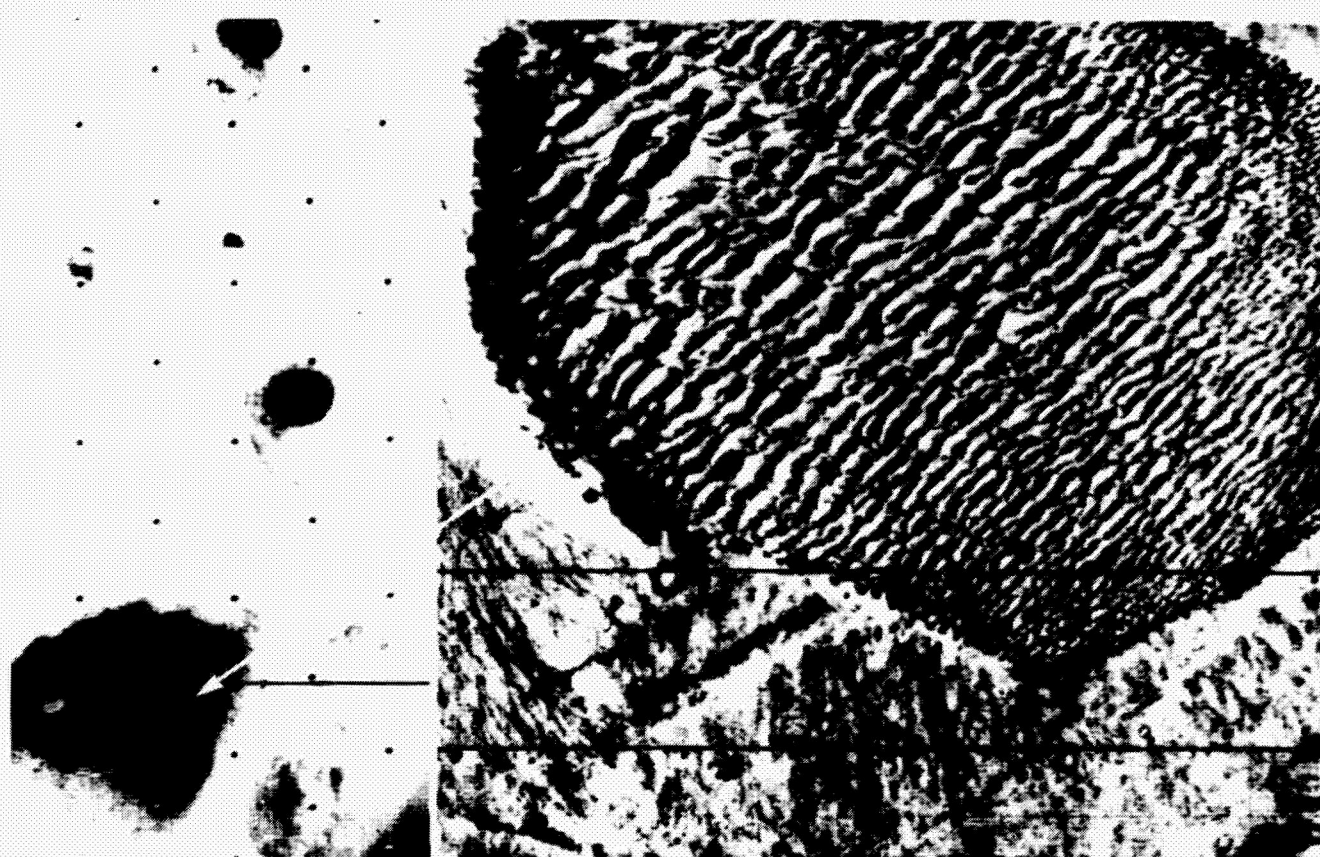


Fig. 36. The wave-like surface texture of the dark patch in the crater, shown in the wide-angle picture (left), can be seen in the adjacent narrow-angle photograph (right). The pattern is indicative of sand dunes. The crater (47°S, 330°W) is about 65 kilometers (40 miles) wide.

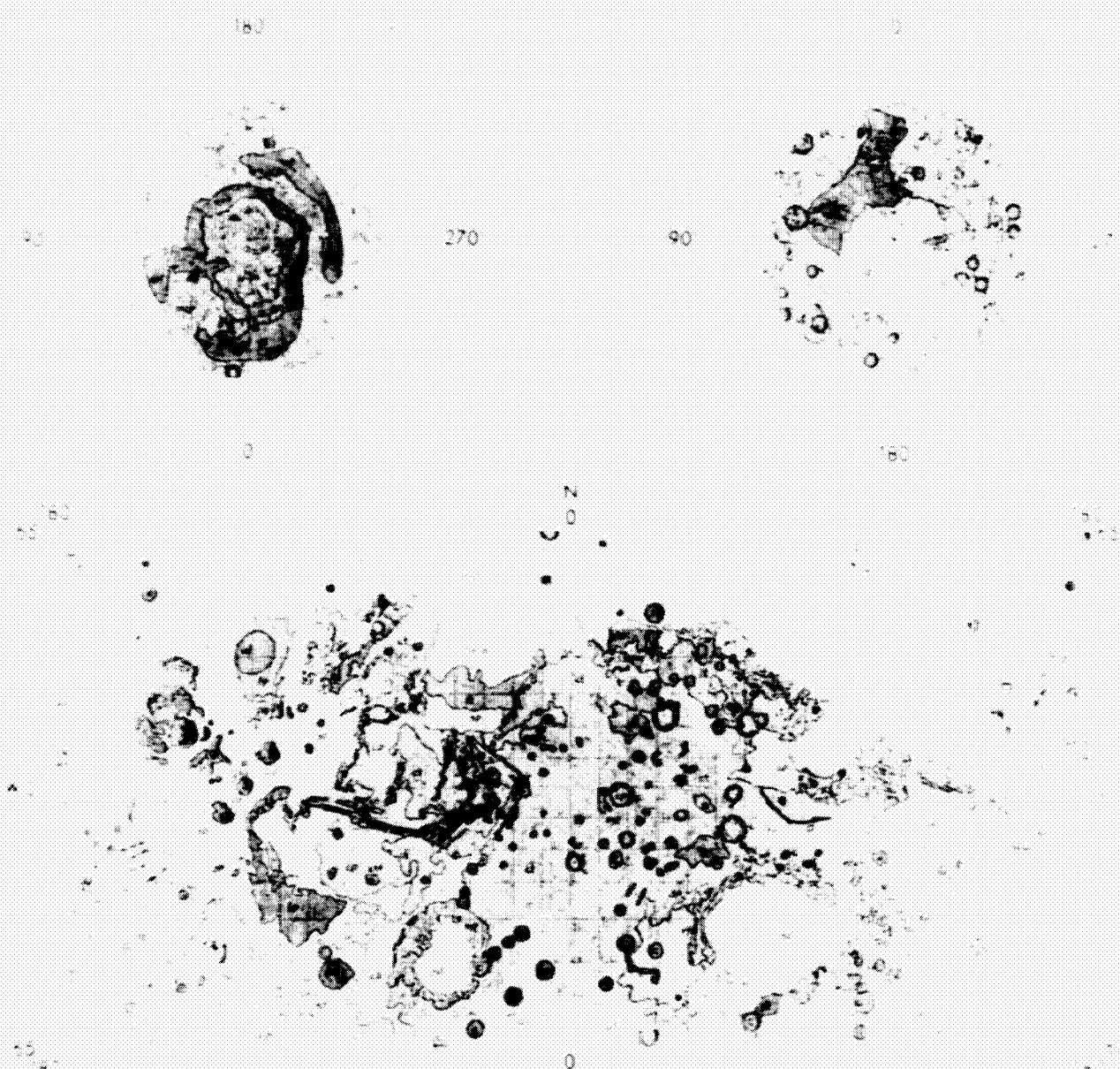


Fig. 37. This preliminary geologic map of the Martian terrain, developed by the U.S. Geological Survey, provides graphic evidence of the variations in the planet's surface.

Spacecraft tracking data indicate that Mars has a unique gravity field (Fig. 38) with variations much more pronounced than those of Earth. The Tharsis Ridge, which contains the four giant volcanic mountains and rises 8 kilometers (5 miles) above the surrounding terrain, is coincident with the largest Martian gravity variation (Fig. 39). From the distribution of

the gravity field and the shape of the planet, it is known that Mars has a preferred axis orientation in the equatorial plane, a natural triaxiality: the spin axis and a major and minor axis in the plane of the equator. The gravity variations measured are as much as 17 times greater than the largest variations measured on Earth.

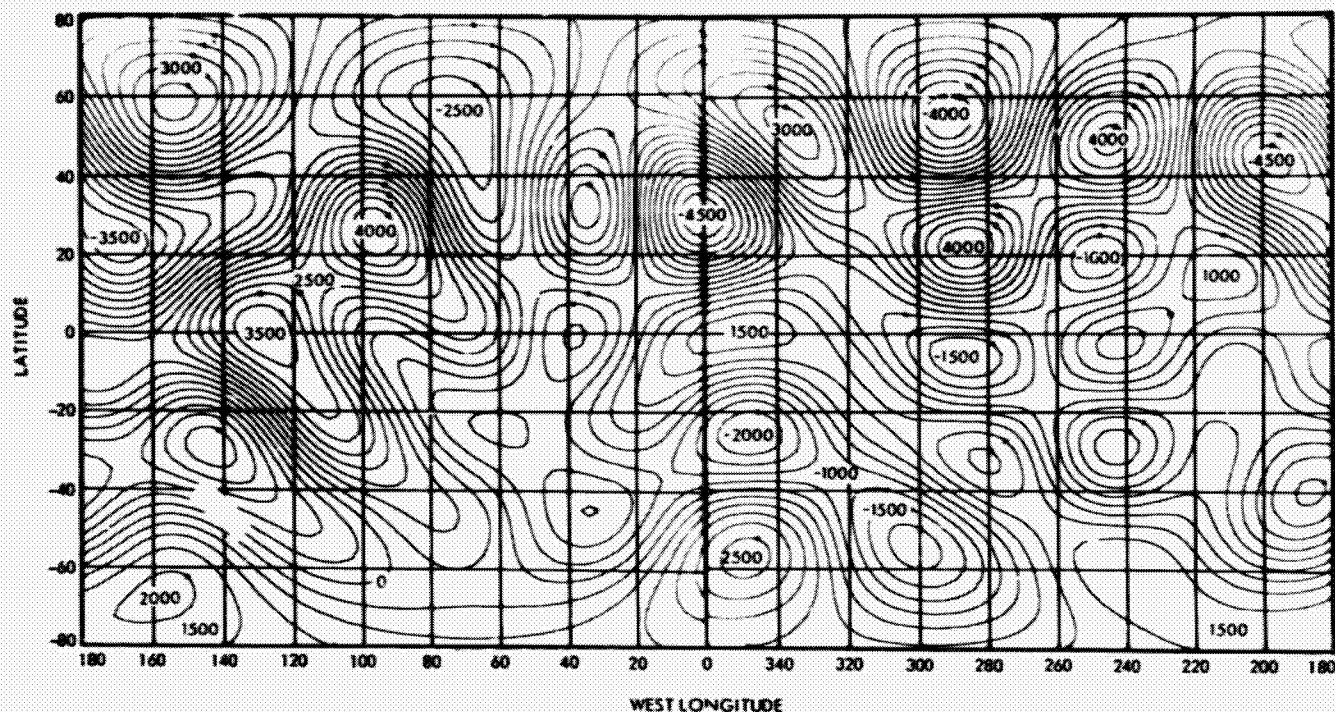


Fig. 38. Surface height contours in meters, corresponding to a gravity field model. The contours indicate the height difference necessary for a surface with uniform density to produce the gravity variation measured. The positive numbers indicate the surface is higher; and minus numbers, lower than the mean radius.

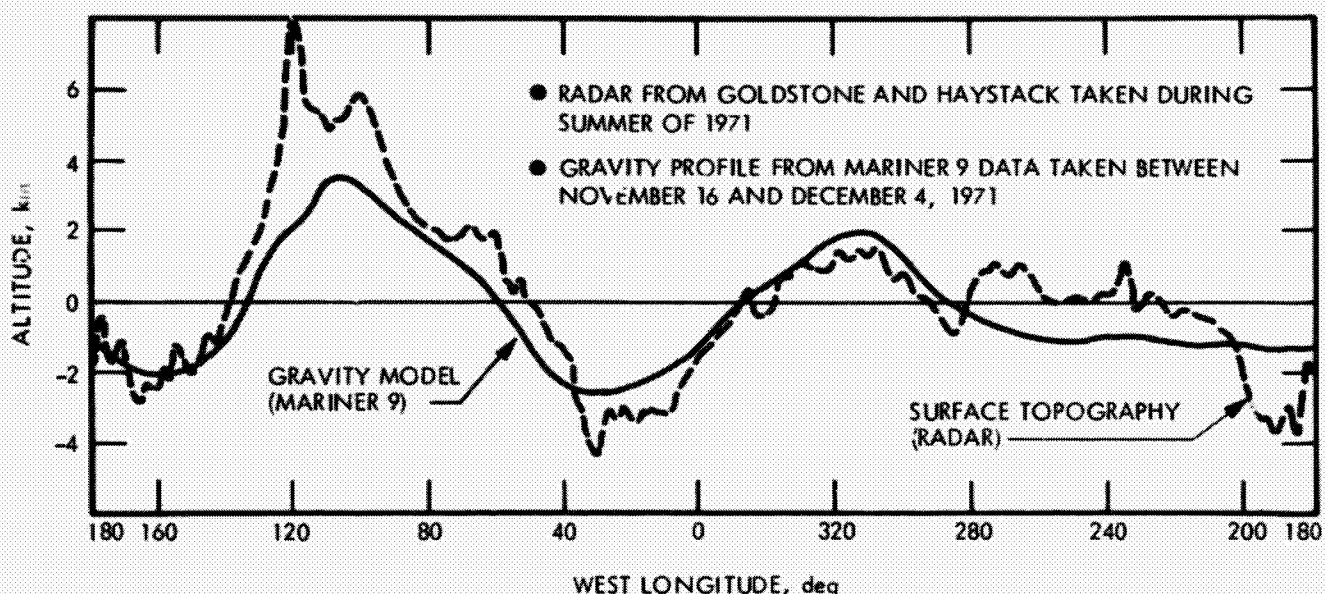


Fig. 39. A comparison between the height at 15°S latitude, calculated from the gravity model (Fig. 38), and the actual elevation measured from earth-based radar. The difference between the two profiles indicates that surface density is probably not uniform.

Atmosphere

The dust storm, which made surface investigation impossible during the early part of the mission, did provide immediate data about the atmosphere of Mars. From the first measurements, some structure could be seen in the upper extreme of the dust pall, revealing a large wave formation extending from the four dark spots to more than 1000 kilometers (600 miles) to the southwest (Fig. 14). When the storm cleared, the wave formation was seen to be associated with the Tharsis Ridge.

Some measurements were made during the peak of the dust storm, when the material entrained in the atmosphere could be sensed by the infrared spectrometer (Figs. 40 and 41). From these measurements, it was determined that the material was probably about 60 percent silicon dioxide, consistent with dust originating from basaltic rock. Surface characteristics measured later, when the atmosphere was clear, indicate a similar silicon dioxide composition, consistent with the ample evidence of volcanism.

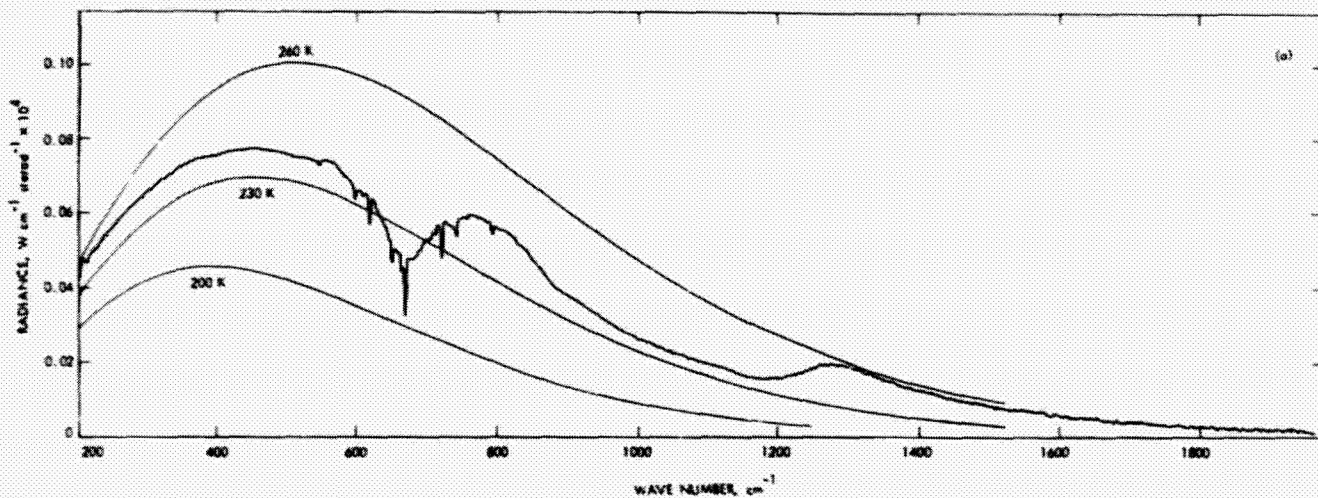


Fig. 40. An example of thermal emission spectra of the south polar cap, measured with the infrared interferometer spectrometer (IRIS). Six individual scans from orbits 29 and 30 are averaged to give this one spectrum. The smooth curve is a profile from a uniform thermal emitter (black body) over the spectral wave-number range. Deviations of the wave numbers from 200 to 500 are influenced by water (H_2O); wave numbers from 400 to 600 and from 850 to 1250 are influenced by the surface composition (SiO_2); and wave numbers from 540 to 800 are influenced by the atmosphere (CO_2).

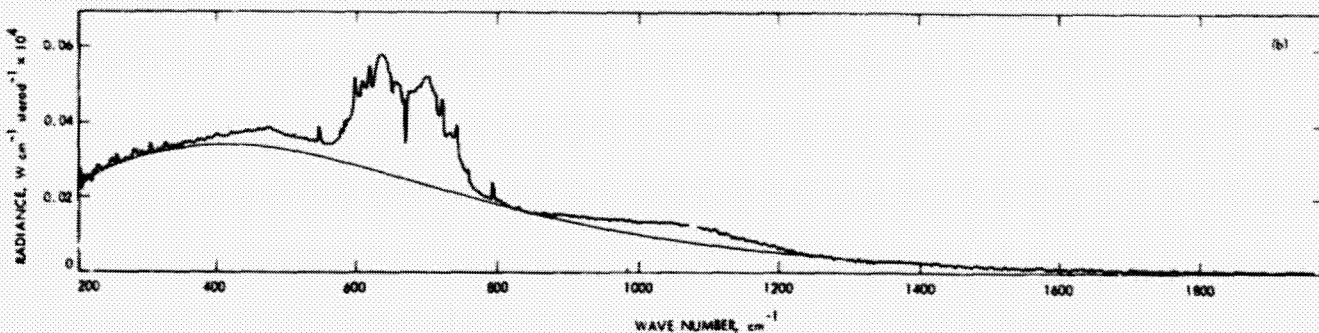


Fig. 41. An example of non-polar thermal emission spectra measured with IRIS. Six individual spectra are averaged from orbit 8 in the region of 18°S, 13°W. Variations from the black body reference curves are influenced by H_2O , SiO_2 , and CO_2 as indicated in Fig. 40.

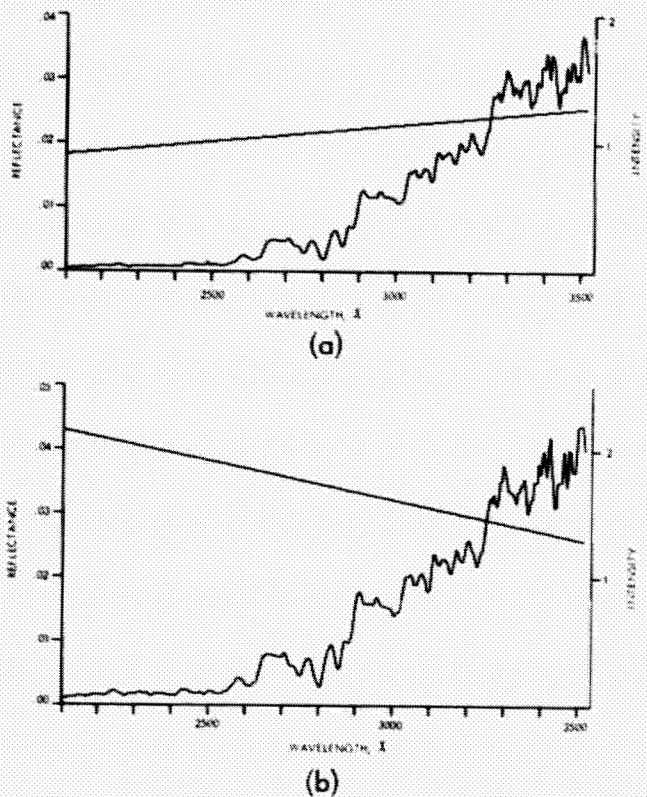


Fig. 42. Ultraviolet reflectance measurements for a dusty region (top curve) and in a relatively clean region (bottom curve) in south pole at latitudes of 45 and 86 degrees, respectively. The irregular curve, increasing in amplitude to the right, is the ultraviolet signal from the Mars atmosphere (intensity, photons $\text{cm}^{-2} \text{ sec}^{-1} \text{ Å}^{-1}$). The straight line indicates the reflectance of the ratio of the intensity of the atmosphere to the intensity of energy from the sun (solar flux). The change in the slope from left to right indicates change in the quantity of the dust in the atmosphere. The heavily dust-laden atmosphere prevented solar energy from penetrating to the lower levels. The low density of the atmosphere above the dust indicated large quantities of dust as high as 15 kilometers (10 miles) above the 6 millibar mean level. Sloping of the line from the peak down to the right signifies atmospheric clearing.

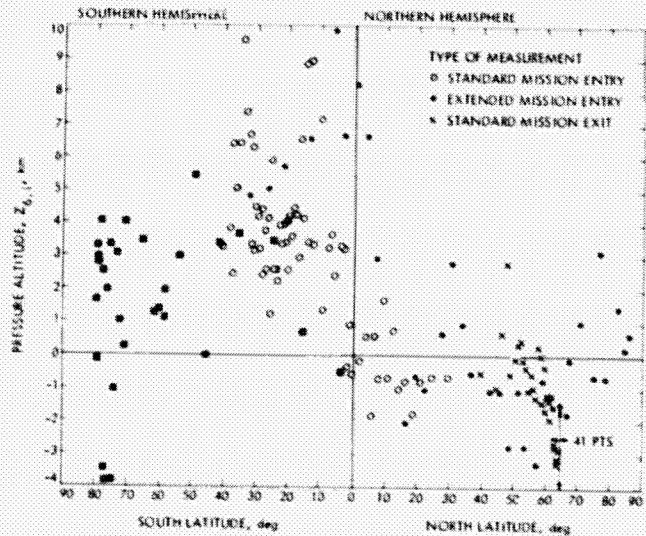


Fig. 43. Results of the radio occultation experiment, which measured the atmospheric pressure at the surface occultation point. The high pressures in the north latitudes indicate a low surface altitude. The surface altitudes in north latitudes are generally lower than in the south by 5 to 6 kilometers. This is consistent with direct radius measurements.

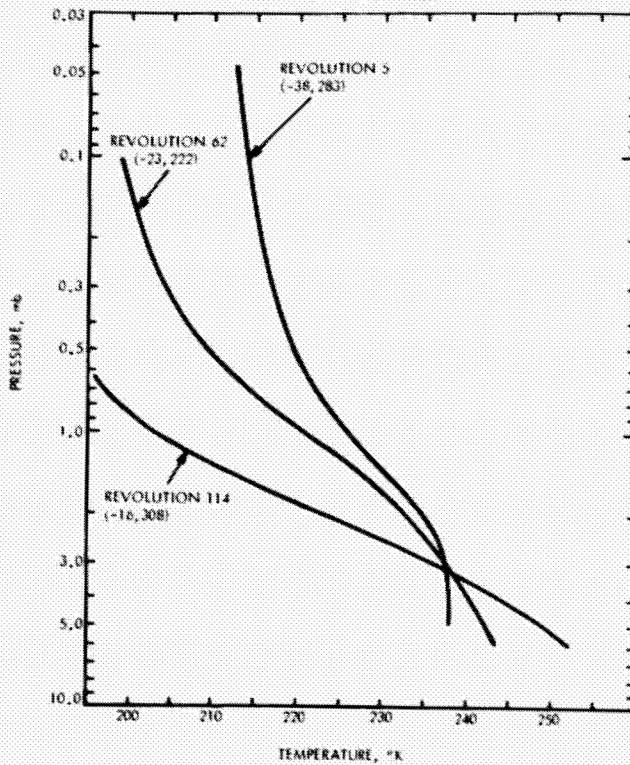


Fig. 44. Representative Martian atmospheric temperature profiles measured by the IRIS. The temperatures go from isothermal (constant with altitude) to almost adiabatic (decreasing with altitude or with reduction of atmospheric pressures). Profiles were obtained from infrared interferometer spectrometer data acquired on November 16, December 14, and January 9.

The depth of the dust pall was estimated from ultraviolet spectrometer (Fig. 42) measurements of the pressure of the atmosphere at the upper boundary and from radio occultation (Fig. 43) and infrared spectrometer (Fig. 44) measurements of the lower boundary (the planet's surface). The average upper boundary pressures were 1 to 2 millibars, which meant the dust was rising 15 kilometers (10 miles) above a mean surface elevation of 6 millibars. In some instances, dust levels as high as 45 kilometers (30 miles) were detected.

The infrared spectrometer and radio occultations determined the atmospheric temperature (Figs. 45 and 46). The temperatures were almost isothermal, i.e., the temperature was constant with altitude, an unexpected but logical result of the dusty atmosphere. As the dust storm subsided, the temperature profiles became more typical, with temperatures decreasing as the altitude increased. Such profiles were also observed by Mariner 4, 6, and 7. From Mariner 9 data, it was noted that the south polar regions had a well-established and well-formed temperature inversion condition (Fig. 47), with the temperature increasing instead of decreasing with altitude for the first few kilometers above the surface.

The more normal condition of temperatures decreasing as the altitude increased (temperature lapse-rate) gave the first

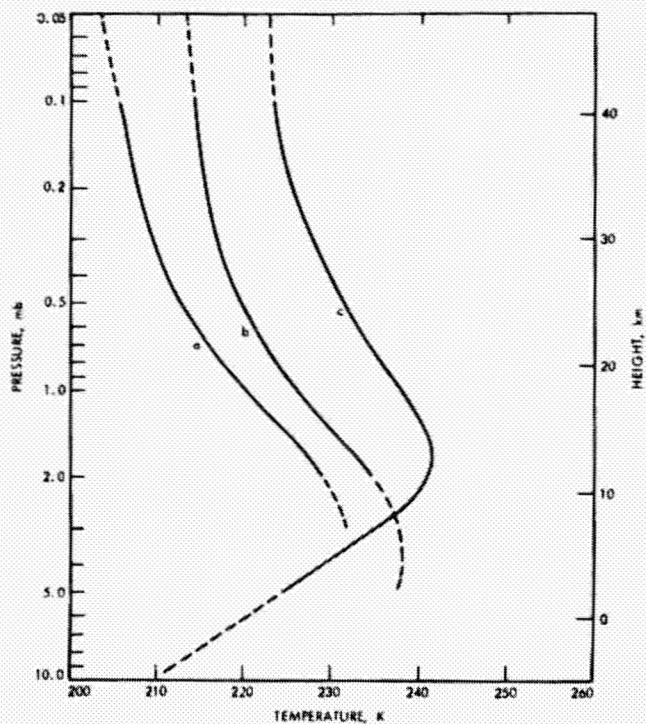


Fig. 45. The temperature as a function of atmospheric pressure level for three locations: (a) 15.0°S , 64.2°W (Sinai); (b) 38.0°S , 282.8°W (Hellas); (c) 86.6°S , 342.2°W (south polar region). The slope reversal on curve (c) is indicative of an inversion layer. Dashed parts of the curves represent uncertain findings. The height scale at right is based on the triple-point pressure of water (6.1 millibars) as a reference.

positive clue that the dust storm was clearing. Ultraviolet spectrometer measurements also showed that the depth of the dust layer was decreasing; ground surface features could be detected, and clearing became evident around the planet. Some areas took longer than others to become visible because of the local winds and/or the denser atmosphere of lower elevations. Hellas, one of the lowest places on Mars, may not have cleared until late in the mission, winter in the southern hemisphere (Fig. 48).

A high-altitude haze (limb haze; see Fig. 49) was observed, as expected, because it had been viewed in the fly-by missions of 1965 and 1969 and also had been predicted from Earth-based observations of cloud movements. Small local dust storms (Fig. 50) were detected on many occasions, and their

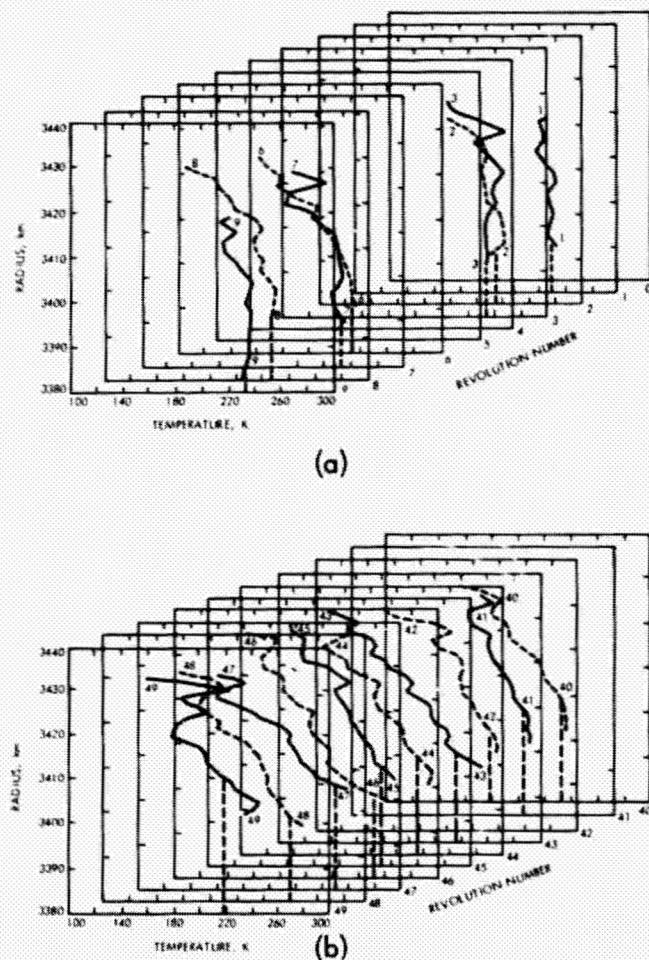
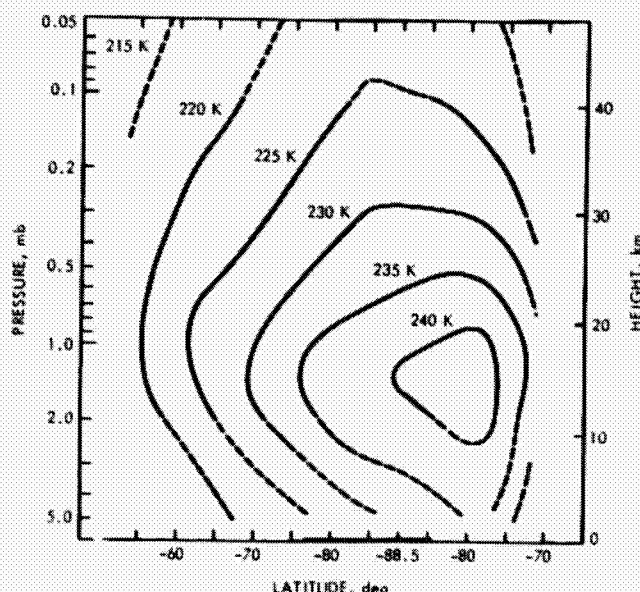
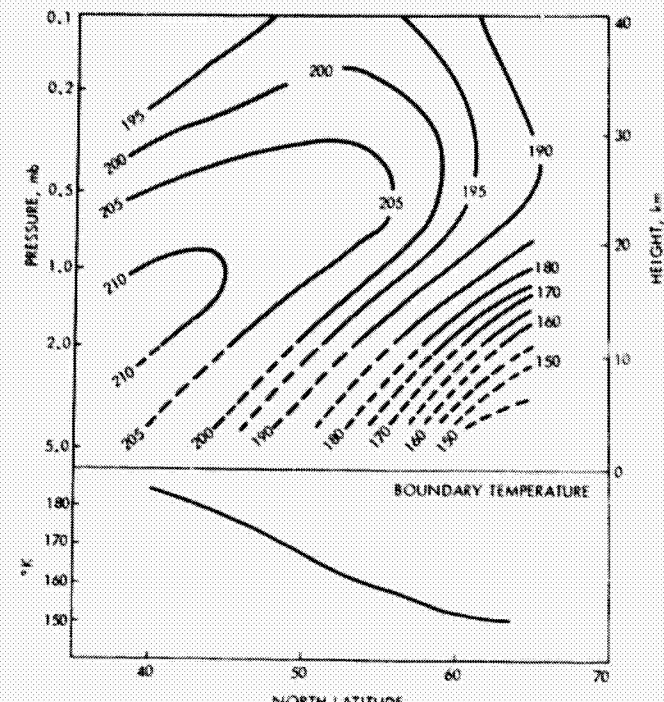


Fig. 46. The atmospheric temperature profiles measured by the radio occultation experiment. The entries for orbits 1 through 9 are shown in (a); entries for orbits 40 through 49 are shown in (b). The lapse rate (temperature change with altitude, radius) is greater for later orbits, when the atmospheric dust began to clear.



(a)



(b)

Fig. 47. Lines of constant temperature (isotherms). (a) Isotherms for a cross-section in the south polar region taken during a single orbital pass by the IRIS. The bar along the abscissa indicates where the south polar cap existed as the scan track approached the south pole. The atmospheric pressure and the height scales are consistent. (b) Isotherms for a cross-section in the north polar region taken on January 3, 1972. The boundary temperature at the bottom of the figure represents the interface between surface and atmosphere.

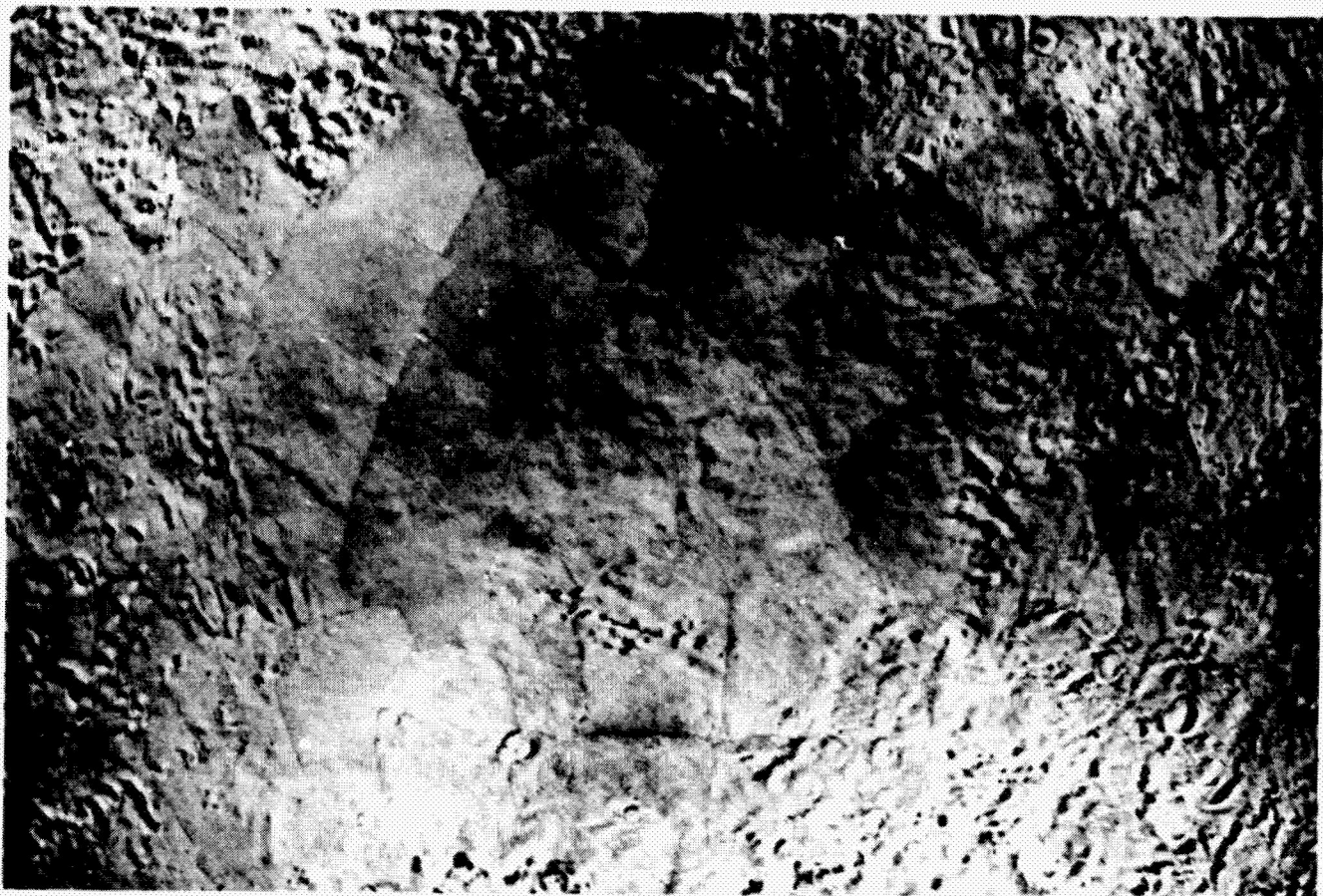


Fig. 48. A part of the mosaicked globe shows the area known as Hellas, 45°S, 290°W. The atmospheric dust, not completely abated at the time of these pictures, obscures the surface detail. Hellas is known to be one of the lowest regions on Mars and, like most low basins, did not become clear until late in the Mariner 9 mission.

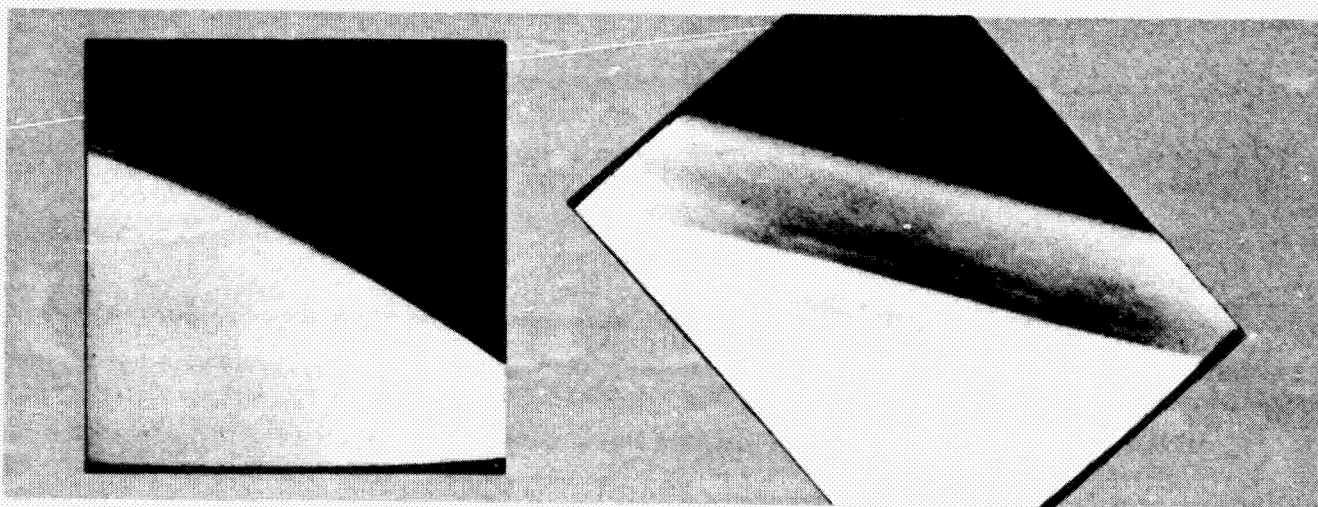


Fig. 49. Limb pictures of the northern hemisphere. The wide-angle picture on the left shows the limb from 45 to 60 degrees with complex cloud layers. The center section of the limb is shown in the narrow-angle picture on the right with ten times better resolution. Two distinct cloud layers are seen. The lower layer is 15 kilometers (9 miles) high; and the upper, about 45 kilometers (28 miles).

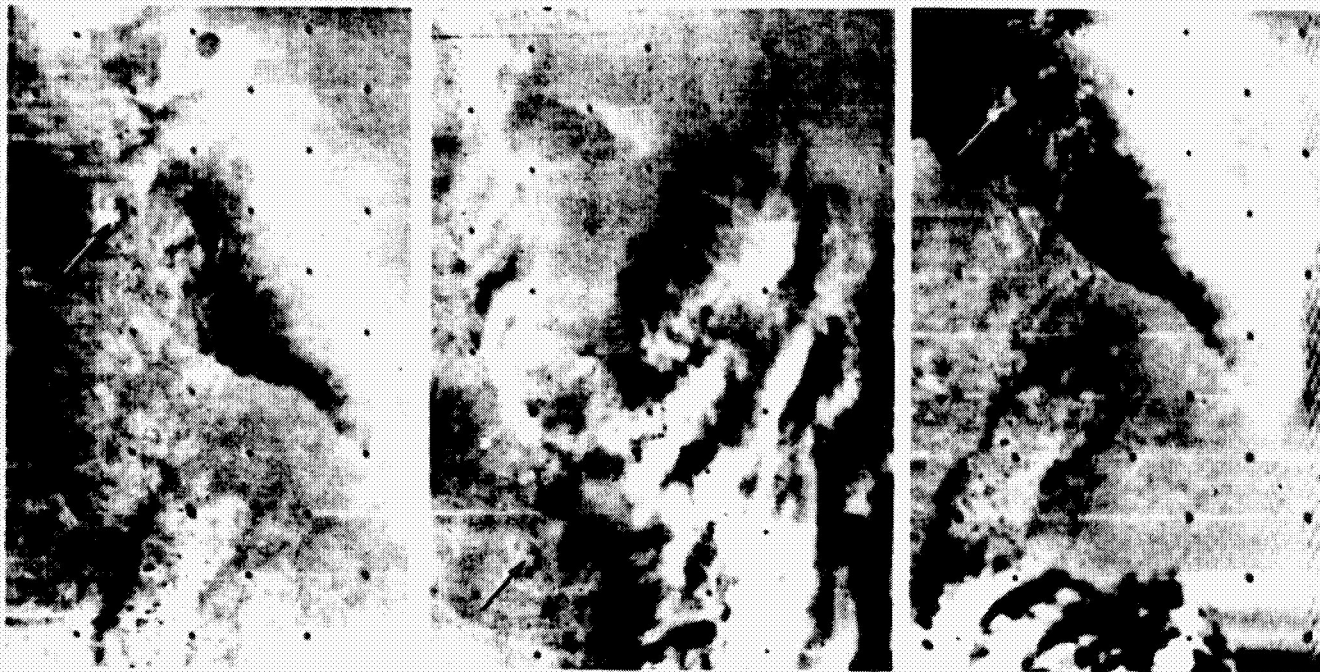


Fig. 50. Two Martian dust storms were photographed by Mariner 9. The photograph on the left was taken February 11; the center picture, about 24 hours later; and the photograph on the right, about two weeks later. The middle picture shows a dust storm 500 kilometers (300 miles) wide. The photograph on the right shows clearing of the central area and, to the left, a new dust cloud about 300 kilometers (190 miles) west of the first storm. The alternate covering and uncovering of dark surfaces by wind-blown light-colored dust is believed to be the cause of the changes in surface markings which have been observed from Earth. The arrows point to the same crater in each photograph.

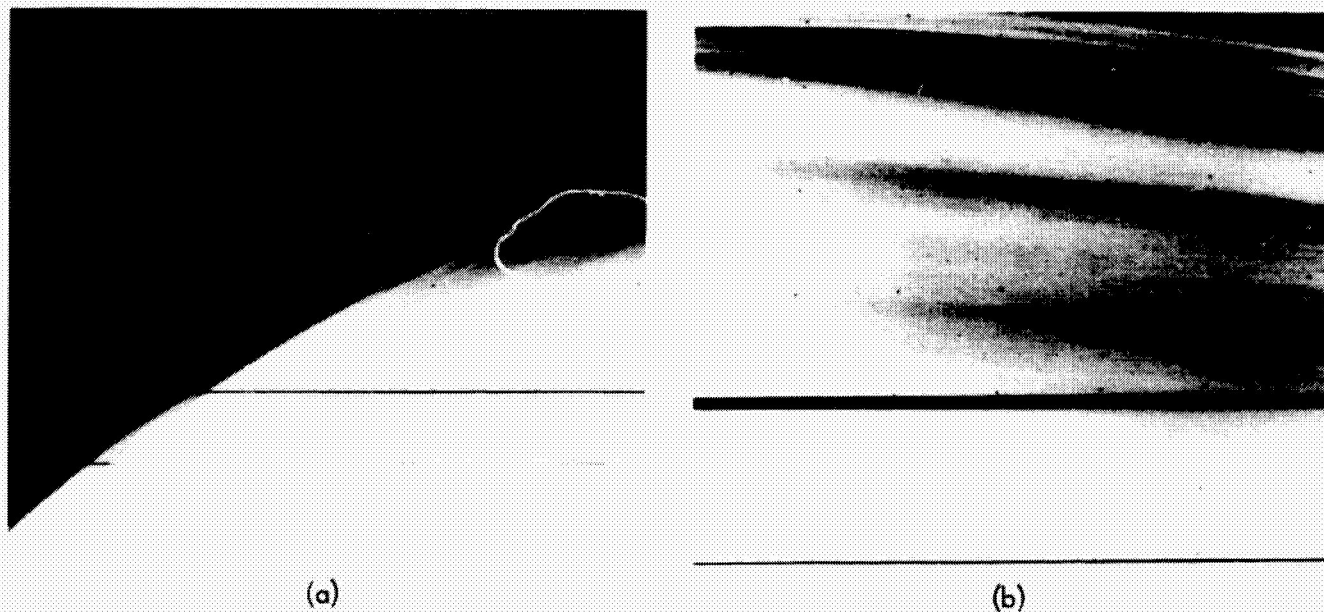


Fig. 51. Cloud layers in the north polar hood. In the wide-angle photograph (left), the limb is seen at the lower left, blending into the terminator (the twilight zone between day and night). The narrow-angle picture (right) shows the detailed structure of the center part of the wide-angle view. The great number of cloud stratifications are revealed by the lighting in the terminator.

motion across the planet's surface monitored. Special priority was given to recording measurements of the polar hood. Mariner 9 found that the hood is not a massive ground-fog formation, as some had speculated, but a complex stratification of clouds (Fig. 51). The many different types of cloud formations, in some cases thin enough to reveal surface features below, have supplied a wealth of new knowledge about the Martian atmosphere.

Cloud formations are both carbon dioxide and water condensation. Massive frontal actions were observed (Fig. 52), and interactions with the underlying topography produced

evident lee wave cloud formations (Figs. 53 and 54). Lee-wave spacing indicated a speed of 200 kilometers (120 miles) per hour. The overall frontal movements show motions of 900 kilometers (500 miles) per day. Winds of higher velocities within the frontal systems are evident because of the dust clouds preceding the frontal-system clouds. Because of the low atmospheric pressure, less than 1/100 of Earth pressure, very high velocity winds are necessary to create enough force to pick up and move the surface dust particles.

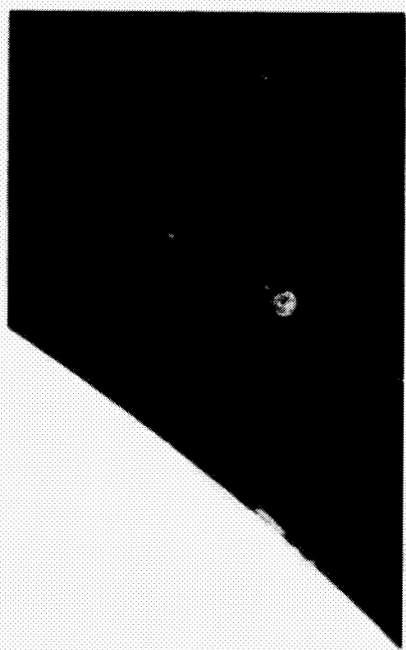
Low-lying cumulus clouds (Fig. 55), moving from the north polar region late in the winter season, were recorded. These



Fig. 52. Atmospheric changes observed on three successive days. The circle in the February 12 photograph indicates the location of the crater visible in the February 13 and 14 pictures. The crater apparently is the summit of a protuberance which causes the perturbations revealed by the cloud patterns.



(a)



(b)

Fig. 53. Thick wave clouds viewed by Mariner 9. On the left, the clouds are viewed in twilight lighting. On the right, special targeting shows the clouds rising above the limb. The cumulus clouds rise several kilometers above the visible cloud blanket. The thin line is a detached haze layer 60 kilometers (37 miles) above the surface.

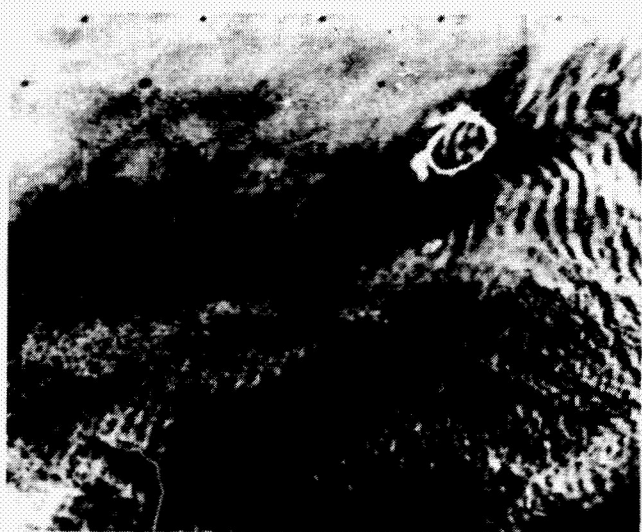


Fig. 54. A crater, similar to that shown in Fig. 52, with a 90-kilometer (56-mile) frost-covered ring at its summit. The perturbation causes a lee-wave pattern in the thinning cloud structure of the north polar hood. At the lower part of the picture, taken on orbit 176, cloud patterns similar to those common on earth are seen spanning an area of 900 kilometers (550 miles).



Fig. 55. A complicated structure in the polar-hood clouds. The central area in the wide-angle photograph (left) is shown in the narrow-angle photograph (right) centered at 60°N, 178°W. The clouds, close to the surface, are similar in appearance to heavy, snow-laden clouds seen on Earth. The wide-angle view spans 1000 kilometers (600 miles), and the narrow-angle picture covers 100 kilometers (60 miles). Both were taken on orbit 214.



Fig. 56. A wide-angle photograph taken on revolution 676, showing brightening of the Tharsis and Nix Olympica regions. The bright areas are massive clouds. With the aid of spectral data from the IRIS, the clouds over Tharsis (bottom of picture) were determined to be water-ice.

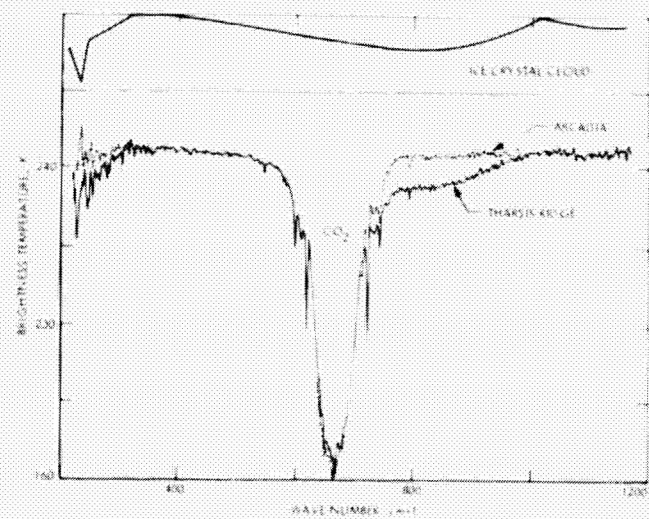


Fig. 57. IRIS spectra taken over the Tharsis Ridge region showing evidence of water-ice in the massive cloud seen in Fig. 56. The difference between the non-clouded region, Arcadia, and the clouded, Tharsis Ridge, follows the same profile as the water-ice spectrum (upper curve), derived in a laboratory.

clouds have all the distinctive characteristics of earthly cumulus clouds heavily laden with snow. Toward the end of the mission, clouds that formed over the Tharsis Ridge and the Nix Olympica area (Fig. 56) were examined by the spacecraft television cameras and by the infrared spectrometer and were found to have the absorption characteristics of water-ice-crystal clouds (Fig. 57).

The composition of the Martian atmosphere is primarily carbon dioxide with small traces of water vapor, but even the small amount of water recorded can produce saturation and cloud formations at the proper temperature and pressure. The heaviest concentrations of water vapor were found to be about 40 to 60 precipitable micrometers (Fig. 58). The precipitable water is the amount of water that can be condensed out of a total column of atmosphere extending from the surface to space. A precipitation of 25 micrometers is about one-thousandth of an inch. Typical readings were about 10 precipitable micrometers, but readings of no measurable water vapor were also common. Other constituents detected were products of carbon dioxide and water vapor (Fig. 59) which had been separated (dissociated) because of the solar flux penetrating the atmosphere. Photodissociation by ultraviolet light causes the separation of the hydrogen and oxygen molecules (Figs. 60 and 61) in water vapor and the dissociation of carbon dioxide, leaving a carbon monoxide and oxygen atom. Variations in the upper atmosphere corresponding to

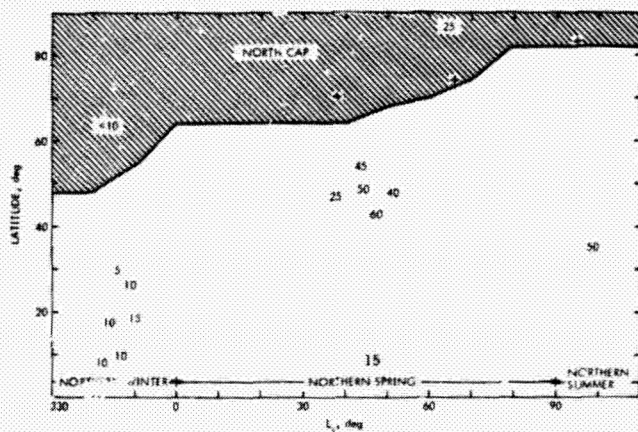


Fig. 58. Distribution of atmospheric H_2O vapor, in precipitable micrometers, for various seasons and regions. Even though these values are low relative to Earth concentrations, they represent a saturated condition for the tenuous Martian atmosphere.

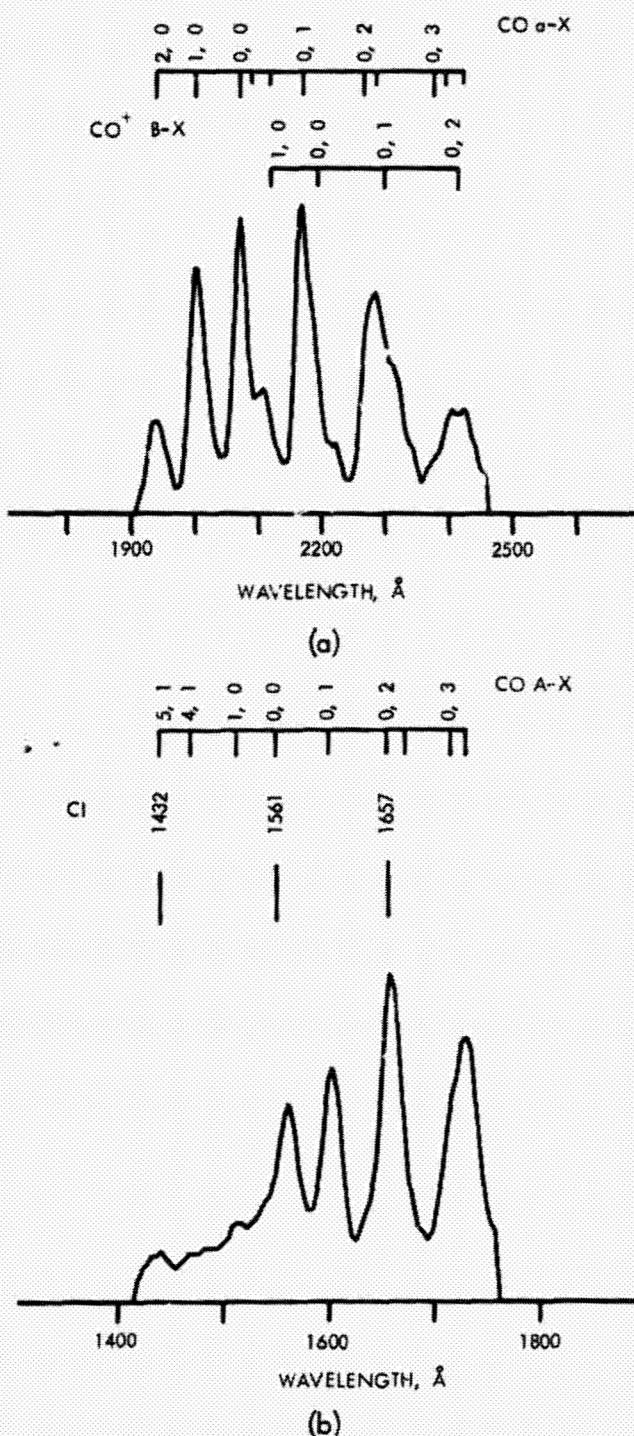


Fig. 59. Airglow spectra (top) recorded with the ultraviolet spectrometer from 2500 to 1900 angstroms (10 angstroms equal 1 nanometer) and from 1800 to 1400 angstroms (bottom). The dissociative excitation of the carbon dioxide, a -X and A -X bands, induced by solar electrons and photons, was used to determine the density distribution of carbon dioxide in the upper atmosphere.

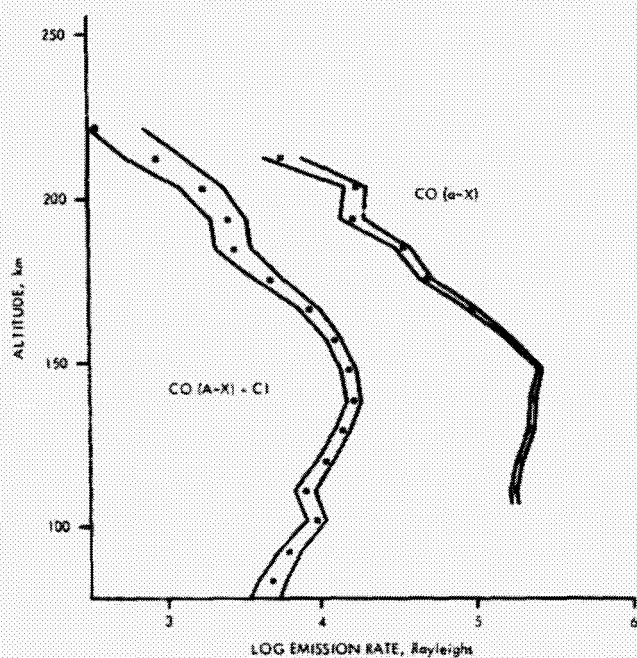


Fig. 60. Emission rate of molecular-gas trace constituents of the atmosphere versus altitude. The carbon monoxide, $a - X$ Cameron bands; the sum of carbon monoxide, $A - X$ fourth positive bands; and the atomic carbon lines are shown as a function of altitude (from limb observations). The dots are data points, and the solid line indicates the standard deviation error of the measurements. The peak emission occurs at an altitude of about 150 kilometers (95 miles).

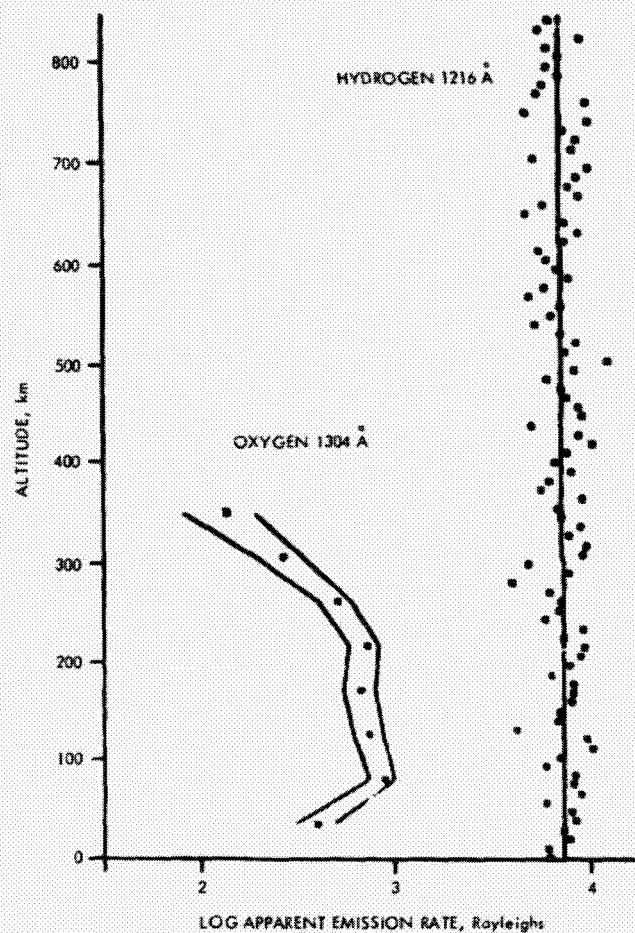
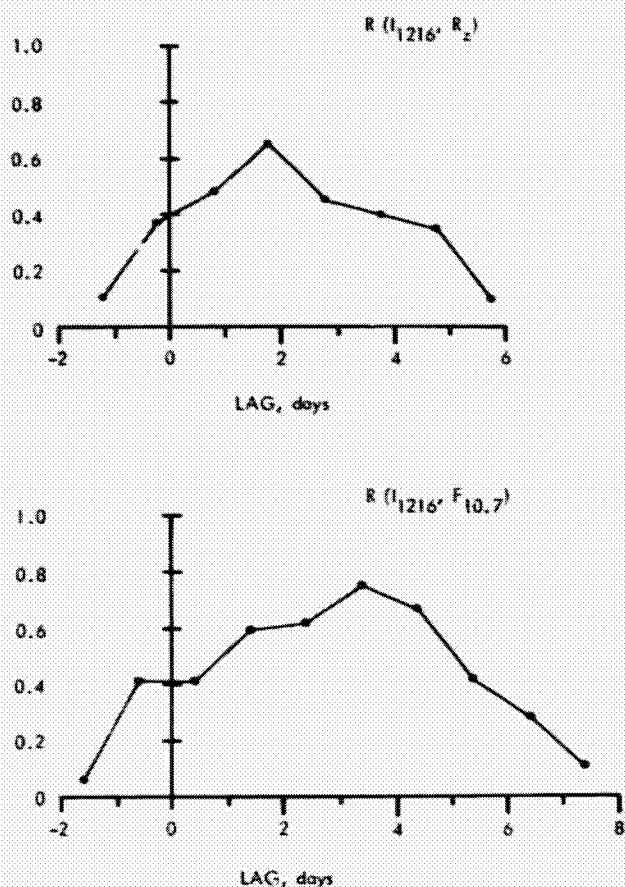


Fig. 61. Emission rates for atomic oxygen and atomic hydrogen. The maximum emission rate for the atomic oxygen occurs at an altitude of approximately 150 kilometers (95 miles). The more energetic hydrogen atom shows an almost constant emission rate as it escapes into space. Escaping hydrogen was detected beyond 20,000 kilometers (12,500 miles), a distance greater than the highest altitude of the Mariner 9 orbit.

the intensity variations of the solar flux (Fig. 62) were also detected. Variations detected in the daytime atmosphere were primarily due to changes in solar activity. Atomic hydrogen, observed by the ultraviolet spectrometer in Lyman alpha measurements, extended many thousands of kilometers as it



CORRELATION COEFFICIENTS OF LYMAN- α INTENSITY (I_{1216}) WITH ZURICH SUNSPOT NUMBER (R_z) AND WITH OTTAWAY 10.7-cm SOLAR FLUX ($F_{10.7}$).

Fig. 62. Solar flux variations for Mars and Earth. The ultraviolet spectrometer was able to determine solar flux variation at Mars by noting the variation in intensity of the Lyman-alpha emission from the hydrogen "cloud" around the planet. The variations at Mars were compared to solar flux variations measured at Earth (Ottawa, Canada). The shape of the profile for Mars and Earth are similar, but, for the early part of the mission, a two-day difference in the time of the occurrence of significant events is noted. The two days correspond to the time it takes the Sun to rotate on its axis from a position where flux coming from a particular longitude on the Sun radiates to Mars and, later, to Earth. Solar activity at Earth could be predicted two days in advance by monitoring the solar flux at Mars with the Mariner 9.

escaped from the planet, in excess of 20,000 kilometers (10,000 miles), well beyond the high point of the Mariner 9 orbit. The hydrogen concentration remained stable, which is an indication that the average amount of water vapor in the Martian atmosphere remains constant. The concentration observed means that about one million gallons of water are dissociated daily, equivalent to enough water to form a layer 6 meters (20 feet) deep, if this process has been continuing for the life of Mars.

Ozone, a three-atom oxygen molecule, has been detected by the ultraviolet spectrometer (Fig. 63) in the polar regions, when they are heavily clouded by the winter polar hood. This seasonal clouding condition starts in late fall and continues for one-half year into late spring or early summer. There have been no detectable ozone measurements when the polar regions are clear.

The search is still continuing for other constituents; at this time, only carbon dioxide, water, and the dissociated components have been found. From the information available, the clouds are either condensates of carbon dioxide, water, or dust.

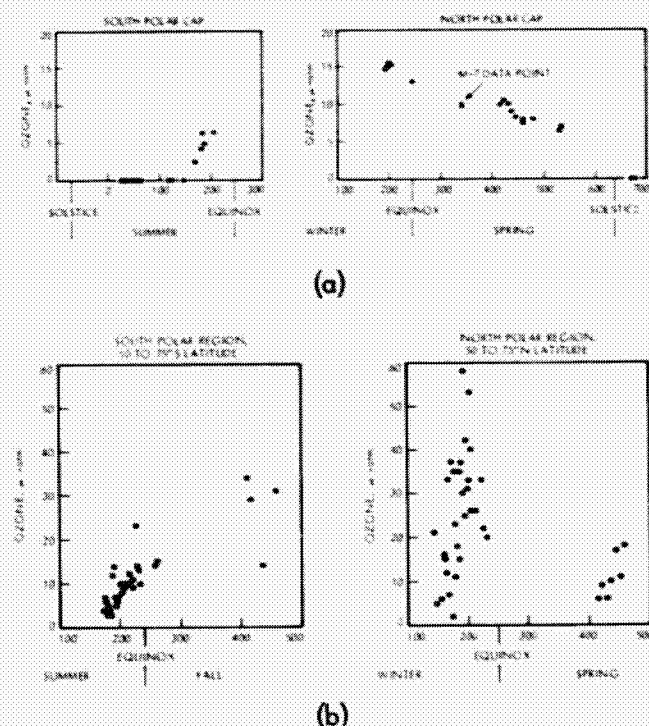


Fig. 63. Ozone measurements. (a) The ultraviolet spectrometer detected the presence of ozone, O_3 , in the polar atmosphere of Mars during the winter and spring when the blanketing clouds (polar hood) were fully developed. (b) The latitudes just below the poles (50 to 75 degrees) also showed a seasonal variation in the ozone measurement.

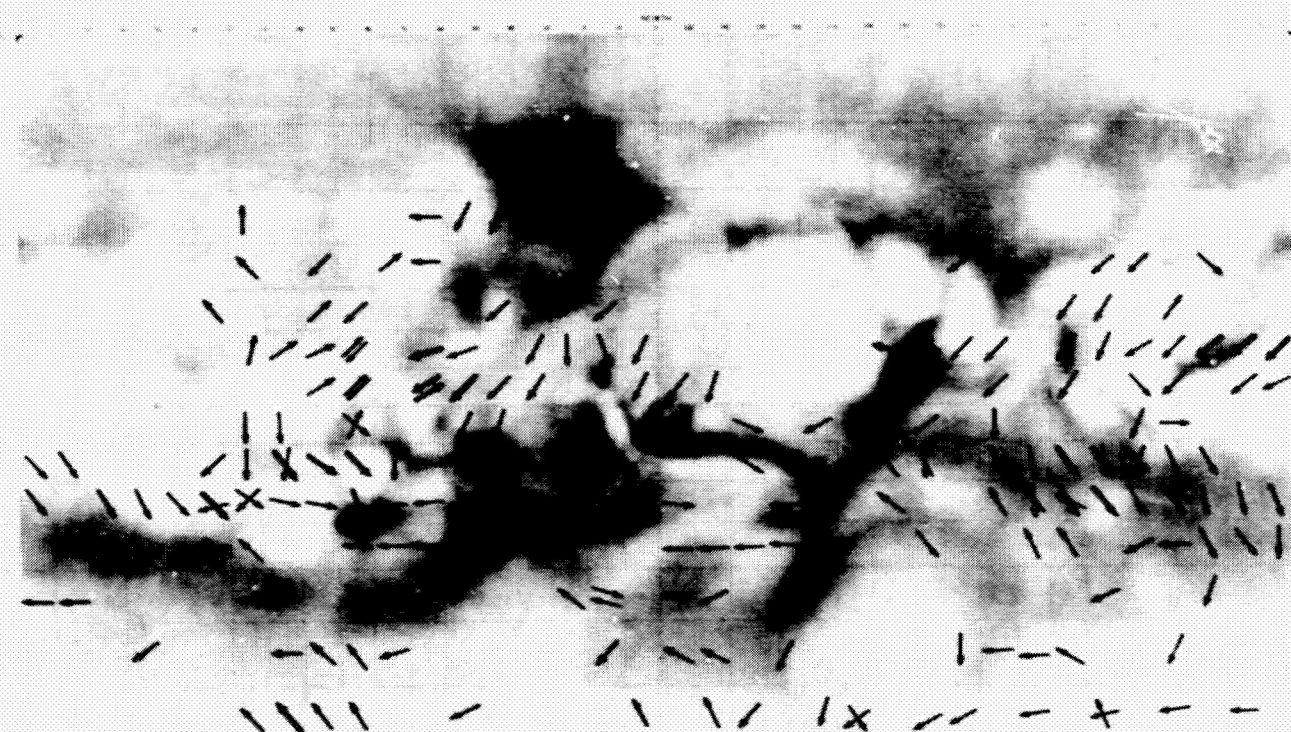


Fig. 64. Preliminary map of prevailing winds. The map, developed from observations of streaks on the surface of Mars, is consistent with measurements of atmospheric pressure by the IRIS and from radio occultations. The wide arrows show areas of heavy streaking.

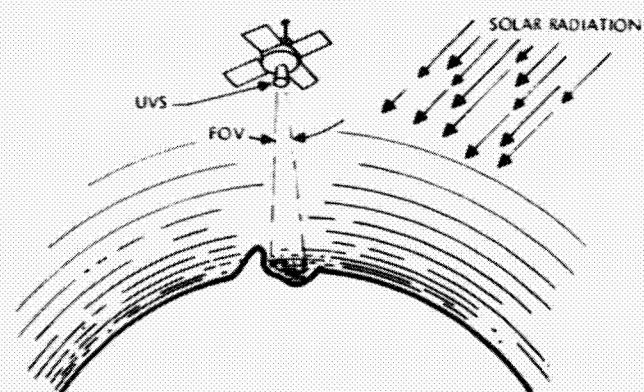


Fig. 65. The intensity of radiation observed by the ultraviolet spectrometer at 3050 angstroms is a function of the number of molecules scattering the incident solar radiation, which, at this wavelength, penetrates to the Martian surface. The lower the surface elevation at which the ultraviolet spectrometer points, the larger the number of atmospheric molecules within its field of view (FOV); consequently, the intensity detected is higher.

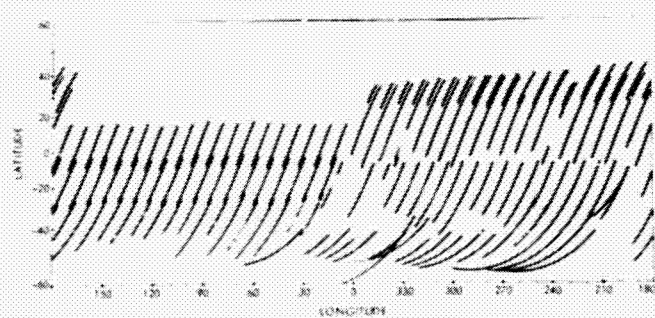


Fig. 66. Latitude and longitude of the 3050-angstrom reflectance measurements by the ultraviolet spectrometer used to construct the pressure-altitude map of Mars.

Variations in the planet's atmosphere are largely associated with daily changes. Some new information about seasonal characteristics was obtained during the six Martian months that Mariner 9 observed the planet. The seasonal characteristics of the south pole have been compared with the seasonal characteristics of the north pole. Similarities have been noted in cap-retreat rate, time when retreat stops, and laminated and etch-pitted terrain. Comparisons between the observations of Mariners 6 and 7 in 1969 and Mariner 9 in 1971 have not shown any long term changes other than the peculiarities associated directly with the dust-laden atmosphere.

Atmospheric pressure profiles, temperature profiles, and winds which would be produced by changes in pressure and temperature have been calculated and compared with observed patterns of wind directions implied by surface streaks (Fig. 64).

The atmospheric surface pressure (Fig. 65), which is used to derive local elevation, was determined from atmospheric measurements by the ultraviolet spectrometer and infrared interferometer spectrometer. The ultraviolet spectrometer measures the light emitted by the atmospheric molecules. Because the spectrometer has a narrow field of view, only a small area can be recorded. These measurements are then averaged to ob-

tain elevations of large areas (Figs. 66 and 67). The infrared interferometer spectrometer measures the absorption by the atmosphere of the energy radiated by the planet. The wide field of view covers a broad area, and the data obtained from each recording provide an area average, but no fine detail. The measurements were used to investigate the volcanic structures on the Tharsis Ridge and the basin, Hellas (Fig. 68). The infrared interferometer spectrometer showed that the largest of all calderas, South Spot, rises about 14 kilometers (9 miles) above its surroundings. One of the ground tracks of the ultraviolet spectrometer passed over the top of Middle Spot (Fig. 69) and the flank of Nix Olympica. The measurements obtained indicate that the peak of Middle Spot rises about 16 kilometers (11 miles) above the surrounding terrain; the surface near the peak of Nix Olympica is 19 kilometers (13 miles) above the foot of the mountain.

The ultraviolet spectrometer was the first instrument to indicate that the "grand canyon" of Mars, the Valles Marineris (Mariner Valley, the name chosen by the International Astronomical Union, August 1973), has elevation variations as deep as 6 kilometers (4 miles; see Fig. 70). Many tracking paths crossed the canyon so that elevation profiles could be developed

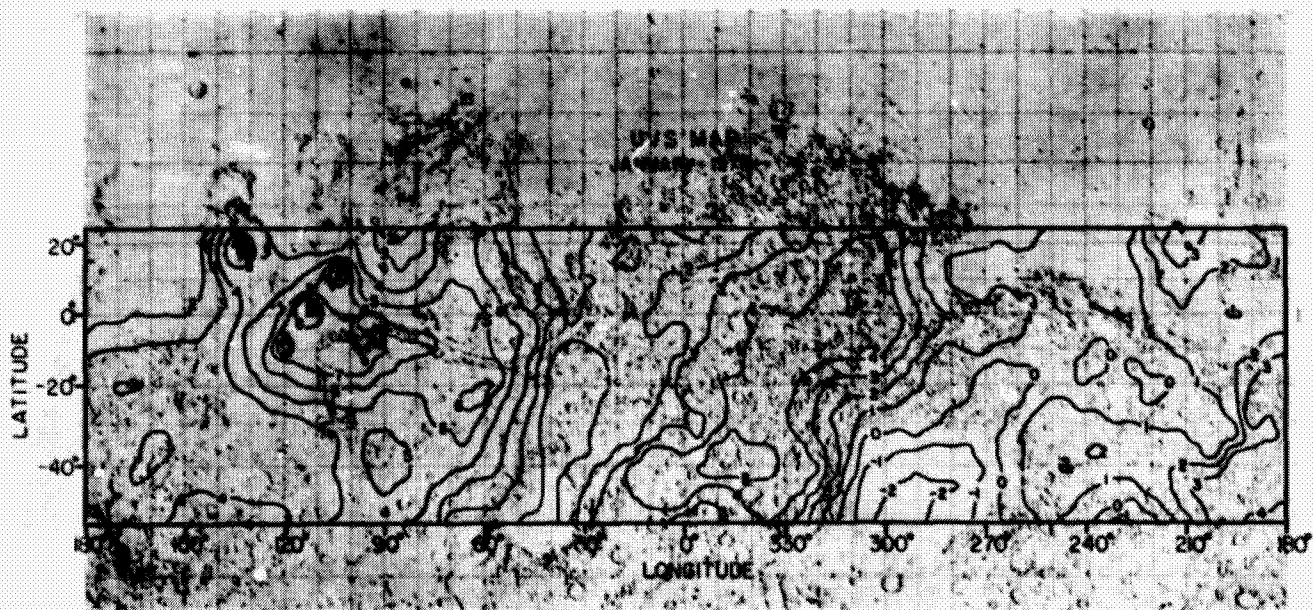


Fig. 67. Preliminary ultraviolet pressure-altitude contour map smoothed to 10 degrees in longitude and latitude. The contour plot is overlaid on a Mercator relief map to show the relation between the geologic features and surface elevations. Nix Olympica, near 130°W and 20°N, and the three aligned, volcanic mountains on the Tharsis Ridge cross the equator at 100°W. The lowest area is located at 290°W and 45°S, a region known as Hellas.

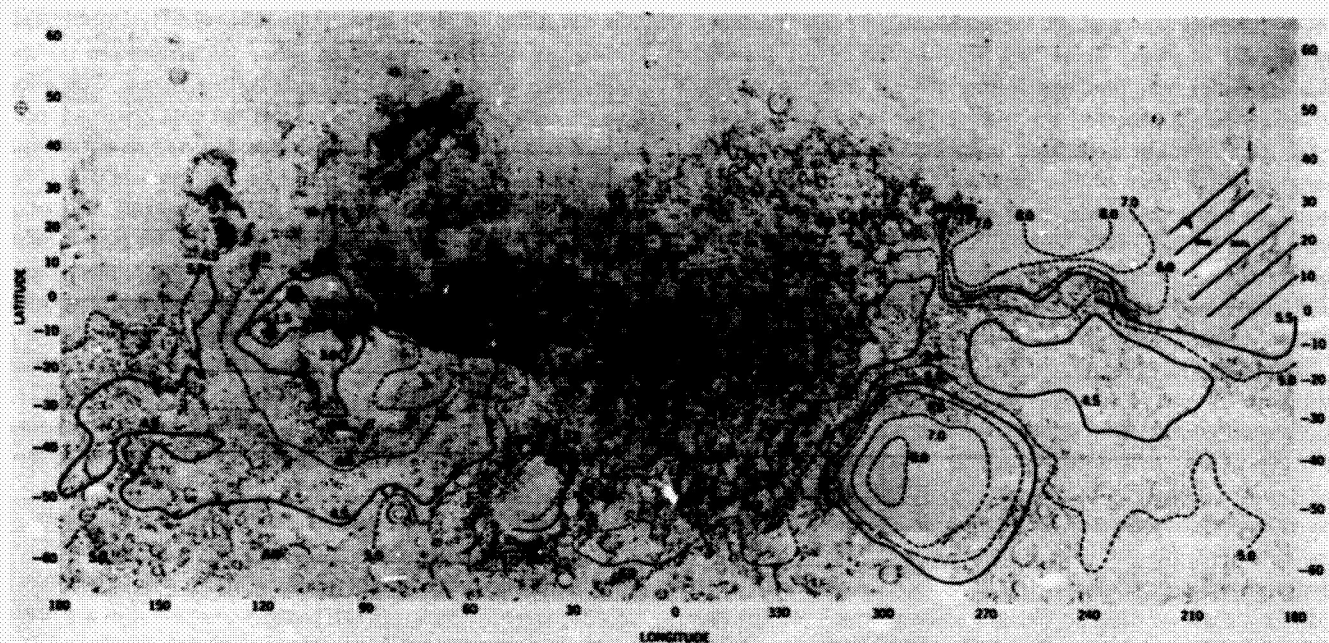


Fig. 68. Surface pressure (pressure-altitude) contour map, derived from IRIS measurements, displayed on the Mercator relief map. The contours represent surface pressure in millibars, with 6.1 millibars at an altitude of 0 kilometer. Pressure increases as elevations become lower and decreases as elevations become higher. Correlation between the ultraviolet and infrared measurements is good.

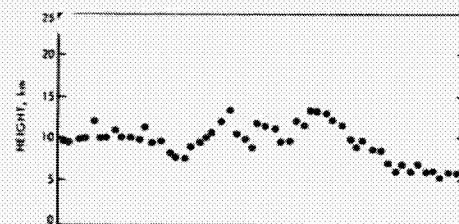


Fig. 69. The elevation variation seen by the ultraviolet instrument in a scan track which went over the volcanic mountain, Middle Spot. At 0 altitude, the surface pressure is 6.1 millibars.

down the length of the 4000-kilometer (2500-mile) canyon. The highest elevation is at the western end of the canyon, where relatively recent fracturing is apparent; the lowest point is to the east. These measurements are important in understanding the appearance of the canyon walls, which seem to

have been modified by a combination of wind and water erosion (Fig. 71). Wind erosion is understandable because winds on Mars exceed 300 kilometers (200 miles) per hour. There also are indications of fluid erosion, with evidence of fully developed channel and river valleys (Figs. 72 and 73).

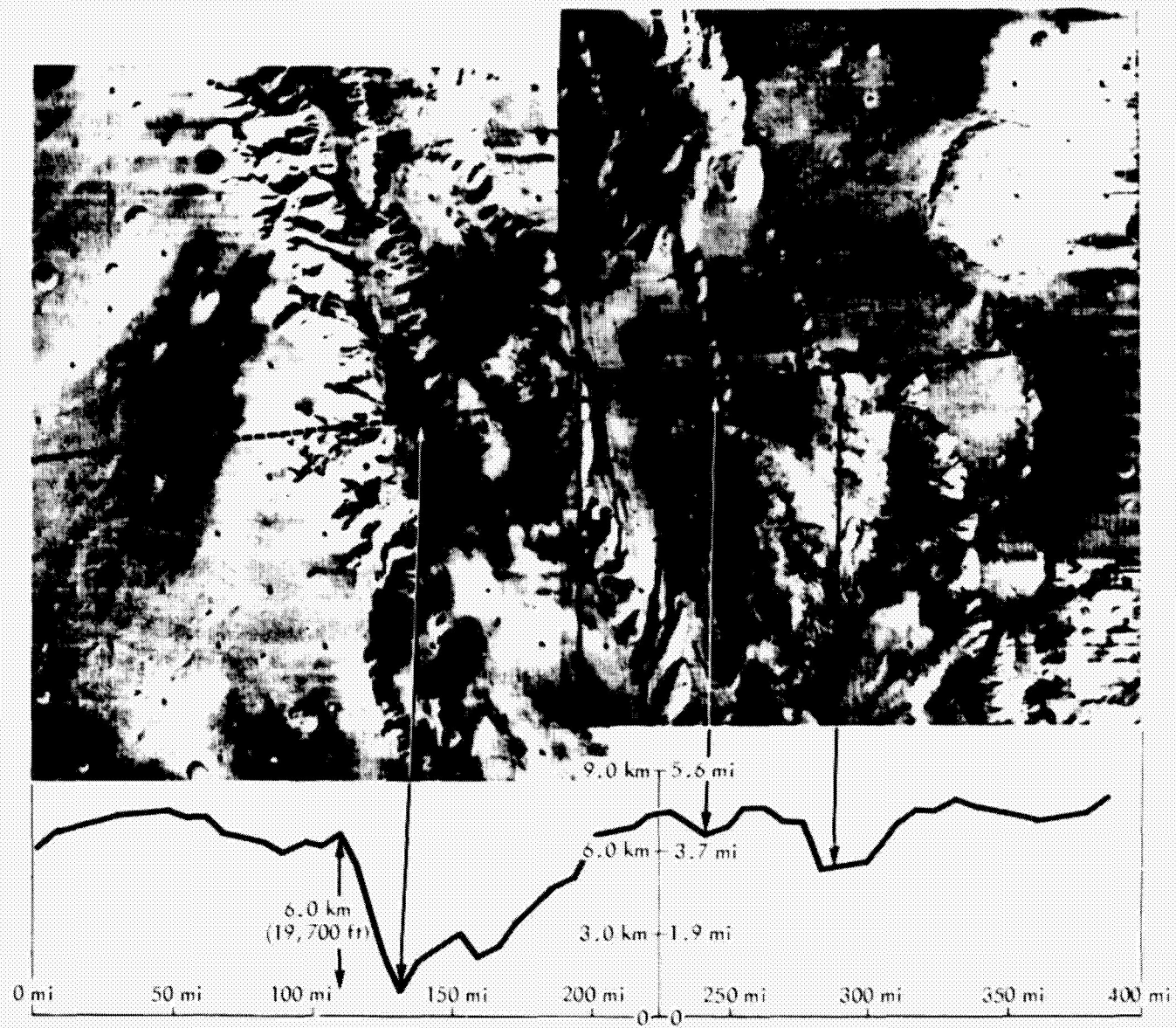


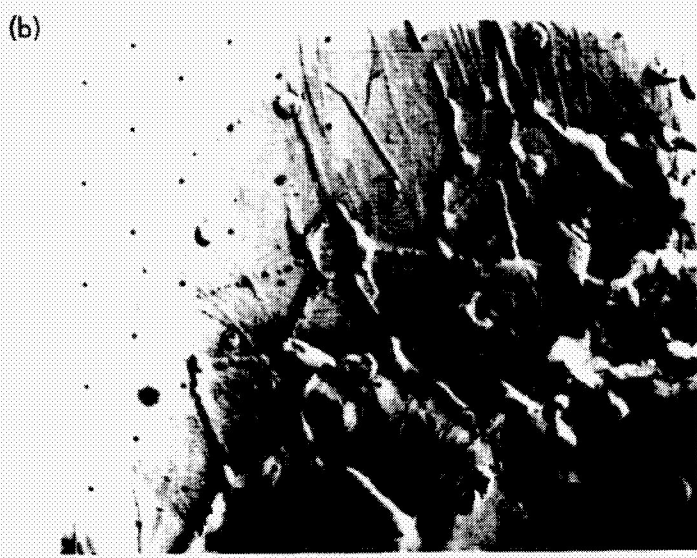
Fig. 70. This mosaic of two photographs of the Tithonus Lacus region on Mars reveals a part of Coprates Canyon four times as deep as the Grand Canyon in Arizona. The pictures were compared with surface pressure measurements made by the ultraviolet spectrometer scan (dotted line). Surface pressure measurements are converted to surface elevations (the profile line below picture). The vast chasma and branching canyons represent a landform evolution apparently unique to Mars. It is believed that subsidence along lines of weakness in the crust and sculpturing by winds formed the features. The photographs taken with the wide-angle camera from an altitude of 1700 kilometers (1070 miles) cover an area 650 kilometers (400 miles) across. North is to the right.



Fig. 71. (a) Panoramic view of the equatorial region. Several hundred photographs, scaled to size, were used in this mosaic. The photographs, taken from late January until mid-March 1972, cover the area from $30^{\circ}N$ to $30^{\circ}S$ and from 20 to $120^{\circ}W$. The volcanic mountains on the Tharsis Ridge are shown upper left. An outline of the United States is superimposed on the mosaic to show the comparative size of the giant canyon, Valles Marineris, extending across the central section. (b) The west end of the canyon, seen in high resolution, lies between San Francisco and Los Angeles. Erosion and stratification of the upper canyon walls, a 'sp' (c), and a mesa (d) can be seen in the central part of the canyon, also shown in high resolution (see Fig. 70 for elevation measurements).



(a)



(b)



(c)



(d)

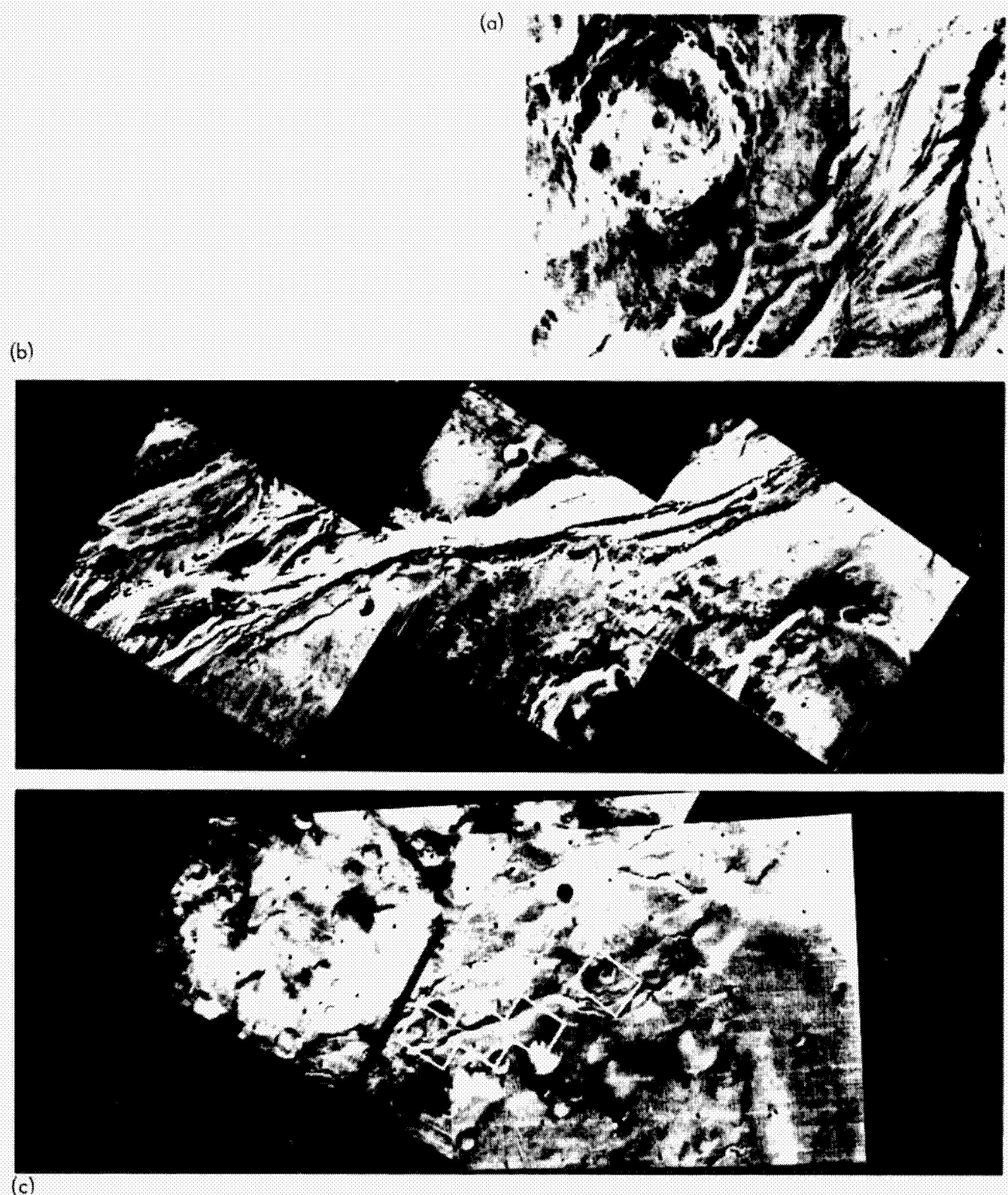


Fig. 72. Channel with braid flow markings. The braid flow is shown in (a), a mosaic of two high-resolution photographs, and in (b), a mosaic of three pictures. The entire channel is shown in (c), a mosaic of two wide-angle photographs. Braided flow is indicative of high density flow which bypasses obstacles and tends to leave a braided appearance in the stream bed.



(a)



(b)

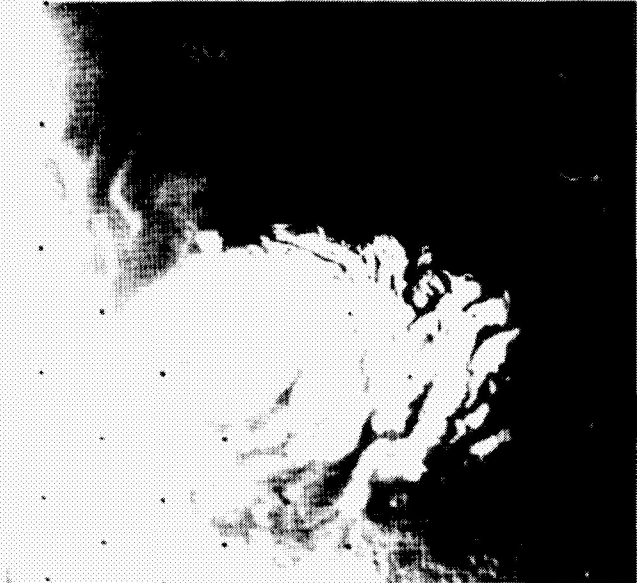
Fig. 73. Two river-like markings discovered on Mars. The larger (a), located in the Rasena region at $182^{\circ}W$, $20^{\circ}S$, is 700 kilometers (435 miles) long. The smaller, located in the Mare Erythraeum at about $40^{\circ}W$, $30^{\circ}S$, is 575 kilometers (355 miles) long. Both features have dendritic tributary systems, which collect into a main channel. The elevation determinations support the apparent flow direction in that the dendritic appearance is in the higher ground.

Computer enhancement of the television pictures emphasizes the otherwise subtle markings of dendritic patterns throughout the equatorial regions (Fig. 74). If fluvial erosion exists, the fluid causing the erosion was probably water. Where are the water sources? Under what circumstances could fluid water have been found on Mars? The present state of Martian atmospheric pressure is not dense enough for fluid water to remain stable. Fluid water exposed on the surface would rapidly evaporate into the atmosphere, cooling the remaining fluid until it had solidified into ice. The water then would remain stable as invisible water vapor in the atmosphere or, if cold enough, as ice.

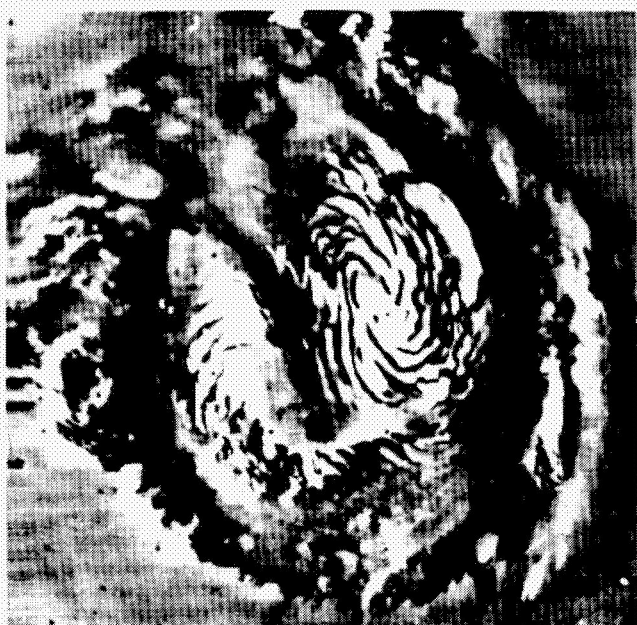
When the features on Mars are examined, there is strong evidence that water might be present as permafrost or subsurface ice. The polar regions are particularly abundant with features that appear to be ice fields (Fig. 75). Whether or not these are water-ice or carbon-dioxide ice, or a combination of both, is still being analyzed. If the water- or carbon-dioxide ice were released by a planet-wide warming trend, the atmosphere of Mars would become considerably more dense than it is now, and fluid water could then be retained on the Martian surface. It is possible that, at some time in the past, Mars had liquid water on its surface.



Fig. 74. Cratered terrain with numerous dendritic patterns revealed by computer enhancement of the photographs. Dendritic patterns are typical of the equatorial regions. The origin of the pattern is unknown, and it will be further investigated in any future missions to Mars.



(a)



(b)

Fig. 75. Terraced structure in the north (a) and south (b) polar caps, photographed late in their respective summers. The terraced structure at both poles and the water-ice on the surface during these seasonal periods indicate that a vast amount of water is stored as ice at the poles of the red planet.

Moons Of Mars

In addition to the vast amount of data concerning Mars, Mariner 9 obtained the first close-up views of the Martian moons, Phobos and Deimos. These moons, first discovered less than 100 years ago by Hall, are too small to be seen other than as a point source by Earth telescopes. Mariner 9 discovered that Phobos and Deimos are irregularly shaped and heavily cratered; they are the darkest objects seen in space.

Phobos (Fig. 76), the moon closer to Mars, is also the larger, 23 by 16 kilometers (17 by 12 miles). Phobos completes one revolution around Mars in only 7.7 hours, a period less than the rotation time of Mars.

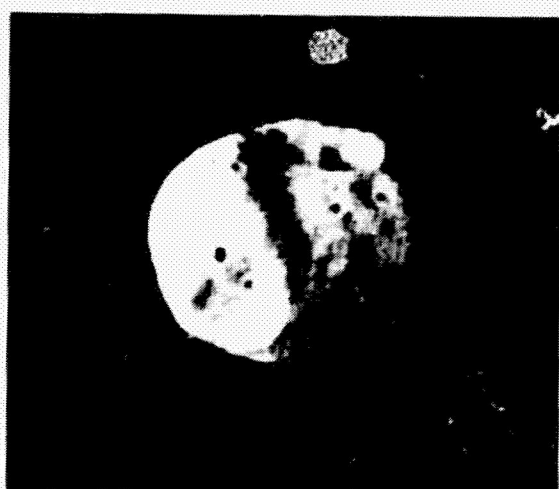
Deimos (Fig. 77) is 13 by 9 kilometers (8 by 6 miles), and has an orbital period of 30.3 hours. Both satellites orbit in a direction from west to east. However, because of the short



DISTANCE FROM SPACECRAFT, 8100 KILOMETERS (5020 MILES); REVOLUTION 77.



DISTANCE FROM SPACECRAFT, 12,500 KILOMETERS (7770 MILES); REVOLUTION 129.



DISTANCE FROM SPACECRAFT, 10,400 KILOMETERS (6460 MILES); REVOLUTION 131.



DISTANCE FROM SPACECRAFT, 5760 KILOMETERS (3580 MILES); REVOLUTION 84.

Fig. 76. Phobos, the inner moon of Mars. Phobos, 23 by 16 kilometers (17 by 12 miles), is the larger of the two moons.

Phobos period, it appears, as seen from the surface, to rise in the west and set in the east, whereas Deimos and the Sun rise in the east and set in the west. Both satellites are in synchronous

rotation, each turning once on its own axis during one revolution about the planet, always keeping the same side toward Mars, much as the Moon does with Earth.



DISTANCE FROM SPACECRAFT: 880 KILOMETERS (550 MILES); RESOLUTION 25.



DISTANCE FROM SPACECRAFT: 772 KILOMETERS (480 MILES); RESOLUTION 65.



DISTANCE FROM SPACECRAFT: 1210 KILOMETERS (750 MILES); RESOLUTION 13.



DISTANCE FROM SPACECRAFT: 347 KILOMETERS (240 MILES); RESOLUTION 14.

Fig. 77. *Deimos, the outer moon of Mars.* Deimos, 13 by 9 kilometers (8 by 6 miles), is the smaller of the two moons.

Conclusion

Mariner 9 completed its mission on October 27, 1972, when its compressed gas supply was depleted, and stabilization, which was maintained by the small gas jets of the attitude control system, could no longer be maintained. The spacecraft slowly tumbled, turning the solar panels away from the Sun, cutting off the necessary operational power. Fifty years may elapse before the orbit decays and the silent spacecraft makes a fiery entrance into the Martian atmosphere and impacts on the surface of the planet.

The information gathered by Mariner 9 has completely changed the concept of the surface and atmosphere of the red planet. Gone are the intriguing questions about the canals

and their intended use, the wave of darkening, and the possibility of seasonal plant growth. A whole new set of questions now exists about this dynamic planet with its active atmosphere, differentiated surface, and variety of geologic characteristics never seen before. Viking in 1976, while providing some of the answers, will undoubtedly pose still another set of questions to be answered by future missions. Mariner 9's legacy to these future explorations is the vast amount of data gathered in its lifetime of 349 days, more data than even imagined by man in all the centuries of Earth-based observations. The complex nature of the red planet is now being revealed by Mariner 9's discovery of the many faces of Mars.

ACKNOWLEDGMENTS

The success of Mariner 9 and the vast scientific results derived from the mission are due to the efforts of many persons. Especially recognized are the significant contributions of the following individuals:

NASA OFFICE OF SPACE SCIENCE: E. W. Glahn, Program Manager; H. Hipsher, Program Scientist; K. Wadlin, Program Engineer.

LEWIS RESEARCH CENTER: D. J. Shramo, Launch Vehicle System Manager.

JPL PROJECT STAFF: D. Schneiderman, Project Manager; J. F. McGee, Assistant Project Manager, Near Earth; E. Pounder, Assistant Project Manager, Near Planet; R. G. Forney, Spacecraft System Manager; R. Laeser, DSN Project Manager; P. J. Rygh, Mission Operations System Manager; N. R. Haynes, Mission Analysis and Engineering Manager; B. C. Houser, Project Control and Administration Manager; R. H. Steinbacher, Project Scientist; A. B. Whitehead, Assistant Project Scientist; T. Vrebalovich, Assistant Project Scientist.

PRINCIPAL INVESTIGATORS: C. A. Barth, University of Colorado, Ultraviolet Spectroscopy Experiment; G. A. Briggs, JPL, Television Experiment; G. de Vaucouleurs, University of Texas, Television Experiment; R. A. Hanel, Goddard Space Flight Center, Infrared Spectroscopy Experiment; A. J. Kliore, JPL, S-Band Occultation Experiment; J. Lederberg, Stanford University, Television Experiment; J. Lorell, JPL, Celestial Mechanics Experiment; H. Masursky, U. S. Geological Survey, Television Experiment; G. Neugebauer, California Institute of Technology, Infrared Radiometry Experiment; I. I. Shapiro, Massachusetts Institute of Technology, Celestial Mechanics Experiment; B. A. Smith, New Mexico State University, Television Experiment.